UPPSALA
UNIVERSITET

Digital Comprehensive Summaries of Uppsala Dissertations from the Faculty of Science and Technology 992

Free Metal Clusters Studied by Photoelectron Spectroscopy

TOMAS ANDERSSON

ACTA
UNIVERSITATIS
UPSALIENSIS
UPPSALA
2012

ISSN 1651-6214
ISBN 978-91-554-8525-2
urn:nbn:se:uu:diva-183031

Dissertation presented at Uppsala University to be publicly examined in 80121, Ångströmlaboratoriet, Lägerhyddsvägen 1, Uppsala, Friday, December 14, 2012 at 10:15 for the degree of Doctor of Philosophy. The examination will be conducted in English.

Abstract
Andersson, T. 2012. Free Metal Clusters Studied by Photoelectron Spectroscopy. Acta Universitatis Upsaliensis. *Digital Comprehensive Summaries of Uppsala Dissertations from the Faculty of Science and Technology* 992. 55 pp. Uppsala. ISBN 978-91-554-8525-2.

Clusters are aggregates of a finite number of atoms or molecules. In the present work, free clusters out of metallic parent materials have been created and studied by synchrotron radiation-based photoelectron spectroscopy. The clusters have been formed and studied in a beam and the electronic structure of the clusters has been investigated. Conclusions have been drawn about the spatial distribution of atoms of different elements in bi-component clusters, about the development of metallicity in small clusters, and about the excitation of plasmons.

Bi-component alloy clusters of sodium and potassium and of copper and silver have been produced. The site-sensitivity of the photoelectron spectroscopy technique has allowed us to probe the geometric distribution of the atoms of the constituent elements by comparing the responses from the bulk and surface of the clusters. In both cases, we have found evidence for a surface-segregated structure, with the element with the largest atoms and lowest cohesive energy (potassium and silver, correspondingly) dominating the surface and with a mixed bulk.

Small clusters of tin and lead have been probed to investigate the development of metallicity. The difference in screening efficiency between metals and non-metals has been utilized to determine in what size range an aggregate of atoms of these metallic parent materials stops to be metallic. For tin this has been found to occur below ~40 atoms while for lead it happened somewhere below 20-30 atoms.

The excitation of bulk and surface plasmons has been studied in clusters of sodium, potassium, magnesium and aluminium, with radii in the nanometer range. The excitation energies have been found to be close to those of the corresponding macroscopic solids. We have also observed spectral features corresponding to multi-quantum plasmon excitation in clusters of Na and K. Such features have in macroscopic solids been interpreted as due to harmonic plasmon excitation. Our observations of features corresponding to the excitation of one bulk and one surface plasmon however suggest the presence of sequential excitation in clusters.

Keywords: clusters, nanoparticles, electronic structure, photoelectron spectroscopy, synchrotron radiation, surface segregation, nanoalloys, size-dependence, metallicity, plasmons

Tomas Andersson, Uppsala University, Department of Physics and Astronomy, Surface and Interface Science, 516, SE-751 20 Uppsala, Sweden.

ISSN 1651-6214
ISBN 978-91-554-8525-2
urn:nbn:se:uu:diva-183031 (http://urn.kb.se/resolve?urn=urn:nbn:se:uu:diva-183031)

List of Papers

This thesis is based on the following papers, which are referred to in the text by their Roman numerals.

I Tchaplyguine, M., Legendre, S., Rosso, A., Bradeanu, I., Öhrwall, G., Canton, S., Andersson, T., Mårtensson, N., Svensson, S., and Björneholm, O. (2009) Single-component surface in binary self-assembled NaK nanoalloy clusters. *Phys. Rev. B*, 80:033405

II Osmekhin, S., Tchaplyguine, M., Mikkelä, M.-H., Huttula, M., Andersson, T., Björneholm, O., and Aksela, S. (2010) Size-dependent transformation of energy structure in free tin clusters studied by photoelectron spectroscopy. *Phys. Rev. A*, 81:023203

III Andersson, T., Zhang, C., Rosso, A., Bradeanu, I., Legendre, S., Canton, S. E., Tchaplyguine, M., Öhrwall, G., Sorensen, S. L., Svensson, S., Mårtensson, N., and Björneholm, O. (2011) Plasmon single- and multi-quantum excitation in free metal clusters as seen by photoelectron spectroscopy. *J. Chem. Phys.*, 134:094511

IV Andersson, T., Zhang, C., Tchaplyguine, M., Svensson, S., Mårtensson, N., and Björneholm, O. (2012) The electronic structure of free aluminum clusters: metallicity and plasmons. *J. Chem. Phys.*, 136:204504

V Björneholm, O., Andersson, T., Svensson, S., Huttula, M., Mikkelä, M.-H., Urpelainen, S., Osmekhin, S., Caló, A., Aksela, S., Aksela, H., Tchaplyguine, M., and Öhrwall, G. Transition to metallicity in small Pb clusters studied by photoelectron spectroscopy. *In manuscript*

VI Tchaplyguine, M., Andersson, T., Zhang, C., Svensson, S., and Björneholm, O. Radially inhomogeneous alloying in self-assembled Cu-Ag nanoparticles—core-shell structure disclosed. *In manuscript*

Comments on my own participation

None of the here presented work could have been accomplished without cooperation. Concerning my own contributions I have taken part in all the experiments; preparations, measurements and the following discussion. In the case of papers III & IV, for which I am the 1st author, I have been the main responsible for the data analysis and the preparation of the manuscript.

The following is a list of publications to which I have contributed, but are are not included in this thesis.

1. Zhang, C., Andersson, T., Svensson, S., Björneholm, O., Huttula, M., Mikkelä, M.-H., Tchaplyguine, M., and Öhrwall, G. (2011) Ionic bonding in free nanoscale NaCl clusters as seen by photoelectron spectroscopy. *J. Chem. Phys.*, 134:124507
2. Mikkelä, M.-H., Tchaplyguine, M., Jänkälä, K.-, Andersson, T., Zhang, C., Björneholm, O., and Huttula, M. (2011) Size-dependent study of Rb and K clusters using core and valence level photoelectron spectroscopy. *Eur. Phys. J. D*, 64:347-52
3. Urpelainen, S., Tchaplyguine, M., Mikkelä, M.-H., Kooser, K., Andersson, T., Zhang, C., Kukk, E., Björneholm, O., and Huttula, M. Experimental observation of large non-conducting antimony nanoclusters – a path towards truly insulating topological insulators? *In manuscript*
4. Zhang, C., Andersson, T., Svensson, S., Björneholm, O., Huttula, M., Mikkelä, M.-H., Anin, D., Tchaplyguine, M., Öhrwall, G. Holding on to electrons in alkali-halide clusters: Decreasing polarizability with increasing coordination. *Submitted*
5. Partanen, L., Mikkelä, M.-H., Huttula, M., Tchaplyguine, M., Zhang, C., Andersson, T., and Björneholm, O. Photoelectron spectroscopy studies of alkali halides in water clusters. *Submitted*

Contents

1. Introduction

1.1. Clusters

Clusters are particles consisting of a finite number of atoms, from 2 and up to ~10^7 [1]. They can be considered an intermediate state of matter, bridging the gap between atoms and small molecules on the one hand and solids on the other. There is no clear limit on the number of constituent atoms that a large assembly of atoms can contain before it is to be considered a solid. Likewise, one can say that there are no general rules stating the number of atoms at which a molecule becomes a small cluster. When clusters are formed, the constituent atoms will strive to arrange themselves in a geometric structure that minimizes the total energy of the system. Which structure this is depends on the type, and number, of incorporated atoms and the type of bonding between them.

Chemical and physical properties of clusters may vary significantly with size. For example, clusters of macroscopically metallic elements may, in some size regime, exhibit semiconductor-like properties. With an increasing amount of constituent atoms the energy bands gradually widen until the band gap eventually disappears and the metal band structure of the solid is reached [2, 3]. From the point of view of fundamental research, clusters are studied to gain understanding of how the properties of solids evolve from those of separate atoms as more and more atoms are bound together.

The possibility to produce particles of specific properties, not only by varying size but also by combining different kinds of atoms in clusters, makes clusters interesting also from the perspective of applied research, e.g. materials science [4]. Another property potentially important for

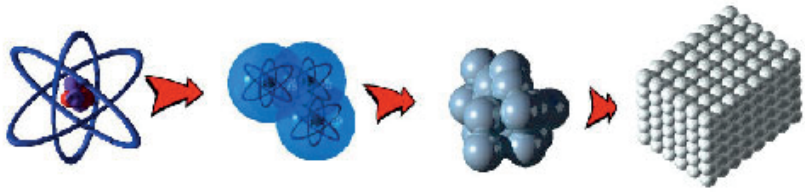

Figure 1.1. Schematic illustration of a transition: Atoms – Molecules – Clusters – Solids.

applications, is the large surface-to-bulk ratio, i.e. the fact that a relatively large fraction of the constituent atoms are situated at the surface. This is not the case in solids where the vast majority of atoms are located in the bulk, without contact with the surrounding medium. Since chemical reactions take place at surfaces, clusters are promising as catalysts [4].

Fundamental natural science, materials science, and catalysis-related research have in general benefited a lot from implementing photoelectron spectroscopy (PES), a unique tool with element- and site-sensitivity, especially suitable in the studies of surfaces. The tuneable x-ray radiation produced at synchrotron facilities provides an optimal way for such studies. The use of PES together with synchrotron radiation in cluster science was for a long time limited to studies of clusters supported on some substrate [5]. The presence of the substrate, however, changes the properties of clusters—both their geometric and electronic structures are influenced. Thus, the inherent properties of clusters can be better understood when looking at free clusters. These can be produced in beams or as aerosols but due to the typically dilute concentrations it was not until the 3rd generation synchrotron radiation facilities came into operation, providing sufficiently intense light of high energy, that the electronic structure of unsupported clusters could be efficiently studied.

1.2. Electronic structure

In the work presented here, free clusters with constituent atoms of metal elements have been studied using synchrotron radiation-based x-ray photoelectron spectroscopy. The electronic structure has been investigated in order to shed light on various properties of the produced clusters.

The electrons bound in a system, e.g. an atom, molecule or solid, occupy a number of discrete states or continuous bands. Those of these levels that have the highest main quantum number, n, for the system are referred to as the valence levels while those of lower n are, as a rule, core levels (in some

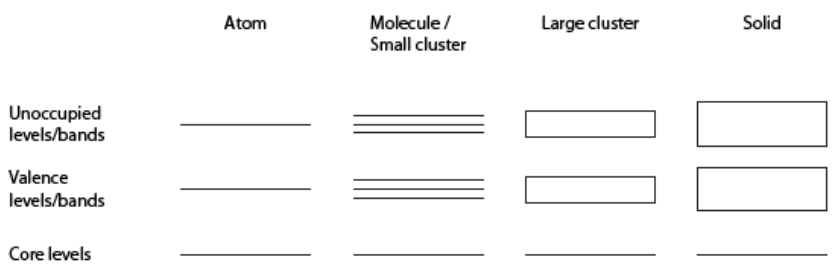

Figure 1.2. A schematic illustration of the principal evolution of electronic structure with size.

cases, like for the transition metal solids also levels with lower main quantum numbers can form the valence bands). The valence electrons determine how a system interacts with its surroundings. As mentioned earlier, clusters can be seen as an intermediate phase between separate atoms/molecules on one side and solids on the other. From this perspective it is helpful to start with a brief repetition of the well-established atom/molecule and solid energy-level structure in order to understand the electronic structure of clusters.

For single atoms, the electronic structure consists of a number of discrete energy levels. When atoms combine into molecules the valence orbitals of the atoms form new molecular valence orbitals participating in the interatomic bonds. These orbitals are as a rule not associated with any specific atom but are distributed over the whole molecule, i.e. they are delocalized. The number of orbitals increases with the number of constituent atoms. The orbitals of the core levels, whose electrons are not involved in the bonding, remain discrete and localized, i.e. they can still be considered to belong to the specific atom to which they were bound before the formation of the molecule.

In solids, the atomic valence orbitals combine to form energetically continuous electronic bands, delocalized over the whole solid. In a simple picture of a ground-state solid, a continuous interval of populated levels formed out of the valence electrons is referred to as the valence band, while the unpopulated set of levels next in energy is called the conduction band. If there is no separation between these two bands, the solid is a metal while if there is a gap, the solid is an insulator or a semiconductor, depending on the gap size (see figure 1.3).

As stated above the core levels maintain their discrete, atomic-like nature also when the atom with which they are associated is part of a larger system, so they do not form bands, but the core-electron binding energies anyway experience significant changes in the atom-to-solid transition, especially for metals. As a rule, the binding energy of a certain core level is several electron volts lower in the solid than in a separate atom of the same element. This is due to two factors, partly due to the cohesive energy, i.e. the energy released in the formation of the solid and keeping the constituent atoms together, and partly due to the interaction of the core vacancy/hole (a positive charge), appearing as a result of the core-level electron removal, with the surrounding atoms. This interaction with the surroundings, often referred to as screening of the core-hole, will be further discussed in section 3.3.

Another characteristic change in the electronic structure of the core-levels is the loss of coupling to the valence electrons, which is a consequence of the valence electron delocalization. In separate atoms and molecules the interaction between the valence and core electrons often causes a rich variety of possible ionic multiplet states, which manifests itself in several different binding energies for the core electrons. In solids, the role of the delocalized

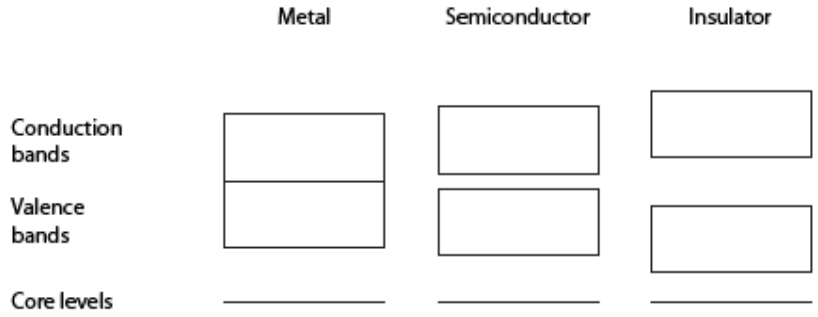

Figure 1.3. A schematic illustration of the principal electronic structure of the solid state.

electrons is limited to just the screening of the positive charge created in the core-level of the probed constituent atom.

For clusters, electronic structure varies with size, between the extremes of a separate atom and a solid. The valence structure goes from the molecular-like discrete orbitals [6] for small clusters towards the solid-like band structure for large clusters [7].Generally, the binding energies of the core levels decrease with size from their atomic to their solid state values. There are, however, some exceptions like, for example, for the halogen atoms in alkali-halide clusters [8].

1.3. Thesis outline

In addition to this introduction chapter, the thesis will continue with the following chapters;

2. descriptions of the two different methods, gas aggregation and the pick-up technique, used to produce free clusters and the equipment involved,
3. a description of the probing technique (electron spectroscopy) used to investigate the clusters, their spectral response, and how the recorded spectra are analysed,
4. the analysis of our experimental results, allowing us to address the spatial distribution of atoms from the different elements in bi-component self-assembled nanoalloy clusters (Papers I, VI), the development of metallicity with size in small clusters (Paper II, V), and the behaviour of plasmon excitations in free metal clusters (Paper III, IV),
5. a summary and an outlook.

2. Methods of cluster production

The clusters in the present studies have been produced through the condensation of metal-vapour atoms. In the studies described in papers I, III, IV and VI, this has been achieved using a so-called gas-aggregation source (section 2.1) while in the work covered by papers II and V, a "pick-up" source (also entitled as the EXMEC (EXchange MEtal Cluster) source, section 2.2) has been used. The vapours of the metals under investigation have been obtained through either resistive or inductive heating of solid samples in dedicated ovens or via magnetron-based sputtering.

2.1. Gas-aggregation source

The schematics of the gas-aggregation source [9] is shown in figure 2.1. Its design is based on that of the Haberland group in Freiburg, Germany [10]. As mentioned above, clusters are formed through the condensation of vapour atoms. As a vapour source, either a resistively heated oven or a magnetron-based sputtering source is used. The oven used in the present experiments consists of a steel cylinder with a so-called Thermocoax heating element [11] wrapped around it. In such an element, in order to electrically isolate the steel cylinder, and the sample, the heating wire is isolated by a ceramic powder kept in place by an outer metal shielding. To reduce the heating of the outer surroundings of the oven, in this case argon gas (see below), the cylinder, along with the wire, is inserted into a container consisting of one ceramic and one steel cylinder. The schematics and a picture of the resistive oven can be seen in figure 2.2. The oven is preferably used to vaporize low

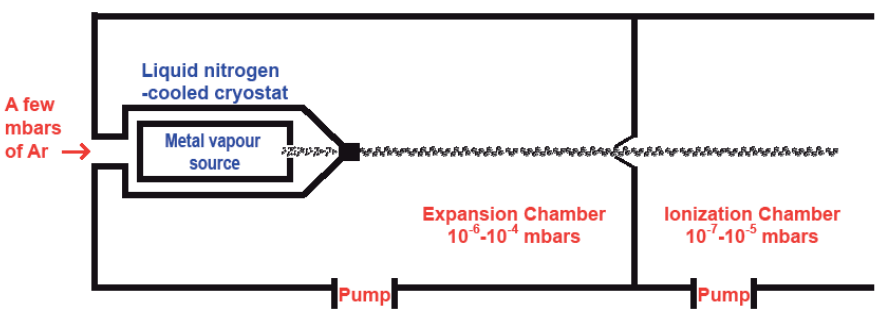

Figure 1.1 Schematics of the gas-aggregation source.

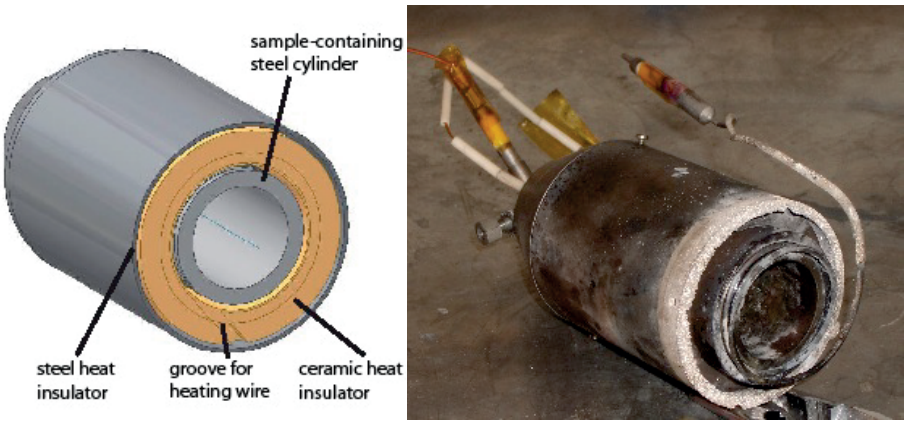

Figure 2.2. Schematics of the resistive oven (left). The oven after having been used to vaporize magnesium (right).

melting point elements, e.g. alkali metals, since their vapour pressures are relatively high already at a few hundred degrees Celsius. For the experiments presented in this thesis, the resistive oven has been used for vaporizing Na, Mg and K. Na and K become liquid before the desired vapour concentrations are reached. The alkali-earth metal magnesium sublimates from the solid phase and demands substantially higher heating than Na and K.

For higher melting point elements, the temperatures that can be reached with the resistive oven are not enough to achieve sufficient vapour pressure. Vapours of these elements may instead be produced through sputtering. Energetic particles (atomic/molecular ions as a rule) accelerated into a surface may, provided that their kinetic energy is high enough, break the bonds of one or a few of the surface atoms and have them emitted—sputtered. In this way vaporization can be achieved.

The sample to be vaporized is kept at a negative potential. When the power is turned on, atoms present in the vicinity of the sample (in our case it is

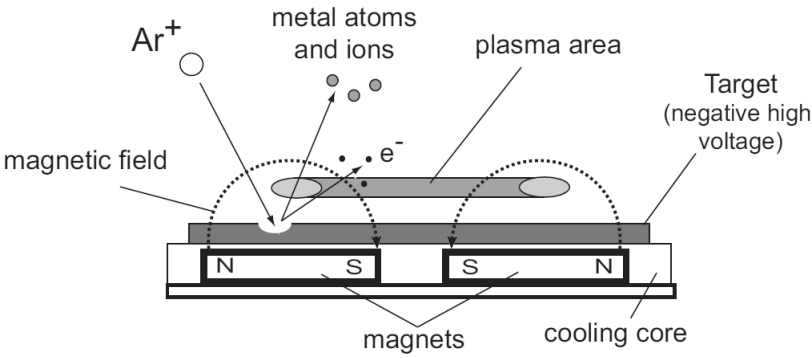

Figure 2.2. Schematic cross-section of a magnetron-based sputtering source. Figure provided by S. Peredkov.

argon atoms) will be ionized and the released electrons will be accelerated away from the sample. The positively charged Ar ions will then be accelerated towards the negatively charged sample and knock out atoms from the surface. The electrons collide with the other atoms and provide their outer shell electrons with enough energy to be ejected. Hence new atoms become ionized and provide further ions for the sputtering process.

To increase the sputtering rate, magnets are placed behind the sample (hence the name magnetron). The magnetic fields will, to a large degree, confine the electrons to the volume just above the sample. The increase in electron density caused by the magnets will increase the number of argon gas ionization events and hence the sputtering rate [12]. With the sputtering source, depending on the applied power and argon pressure, a significant fraction of the outgoing particles can be ionized [13]. In this work, the sputtering source has been used for vaporization of Al, Cu and Ag. The schematics of the magnetron-based sputtering source is illustrated in figure 2.3.

Since atoms are increasingly inclined to condense with decreasing temperature, the vapour atoms should be cooled. The vapour source is placed inside a liquid nitrogen-cooled cryostat (figure 2.4) into which a few mbar of argon is continuously injected. The cryostat is in turn placed inside a vacuum chamber (expansion chamber) where the pressure is 10^{-5}-10^{-4} mbar (during operation). The vapour atoms are effectively cooled through collisions with the cold inert-gas atoms. The argon gas flow continues out from the cryostat into the expansion chamber and carries the clustering vapour atoms along. On the way out from the cryostat the clusters, and the argon gas, passes through a nozzle with a diameter around 1 mm and a length of about 3 cm. The flow through the nozzle increases the condensation additionally. The nozzle also serves to collimate the gas flow into a beam directed towards the experimental chamber (ionization chamber) opening. On its way towards the

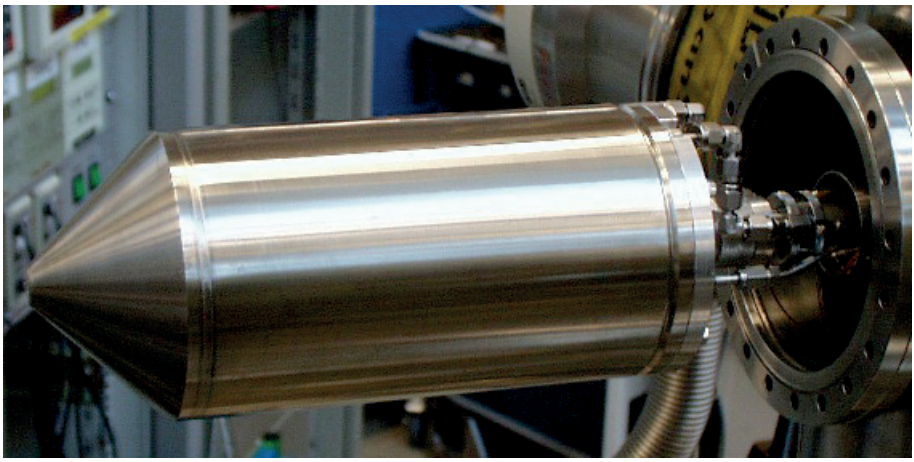

Figure 2.3. The cryostat moved out from the expansion chamber (nozzle not attached).

ionization chamber (a distance of a few cm), the beam passes through a conical skimmer, with a diameter of 1-2 mm, placed at the entrance to the ionization chamber. In this way the clusters are allowed to enter and the stray atoms are rejected.

The size of the produced clusters depends mainly on the metal-vapour and argon pressures, the cryostat temperature and the nozzle geometry. Atoms of different elements are differently inclined to form clusters. For the work presented here the cluster sizes vary between ~10^3 atoms for sodium to ~10^5 atoms for magnesium. In the beam there is a size distribution around some mean number of constituent atoms, $< N >$. In the present type of experiments with the gas-aggregation source in question, the range of produced mean cluster sizes, that can be probed, is limited since the cluster abundance in the beam decreases with decreasing size. (Using a different technique, time-of-flight electron spectroscopy with laser ionization, similar gas-aggregation sources have however shown the capability of producing clusters containing down to just a few atoms [14]). The mean radius and number of constituent atoms can be estimated from the photoelectron signal, as will be described in the discussion of the spectral response of clusters in chapter 3.

2.2. Pick-up source (EXMEC source)

The schematics of the pick-up source [15] is shown in figure 2.5. The central idea is to seed metal vapour with a beam of cold Ar clusters, which collect (pick up) metal atoms on their way through the vapour. The picked-up metal atoms agglomerate at the surface/inside of the Ar clusters which gradually, and in the long run completely, evaporate due to the thermal energy transferred from the metal atoms, so that only a beam of assemblies of metal atoms—clusters—remains.

The Ar cluster beam is formed using an adiabatic expansion source, the principles of which have been described in ref. [16]. Ar gas is allowed to expand out through a conical, liquid nitrogen-cooled, steel nozzle into an evacuated expansion chamber (pumped down to 10^{-6}-10^{-7} mbar before the experiments) which causes the argon atoms to aggregate into clusters (the expansion chamber pressure then increases to 10^{-2}-10^{-3} mbar). The resulting beam then passes through a skimmer which, as in the gas-aggregation source, serves to sort out uncondensed Ar atoms and let the formed clusters pass into the ionization chamber. Here the clusters are sent through the metal vapour. The larger the Ar clusters are, the more metal atoms they can pick up, and the larger metal clusters will be formed.

The vapour source is again an oven, but smaller and of another construction than the one used in the gas-aggregation source. The sample to be vaporized is loaded into a detachable cylindrical crucible. At the upper part of

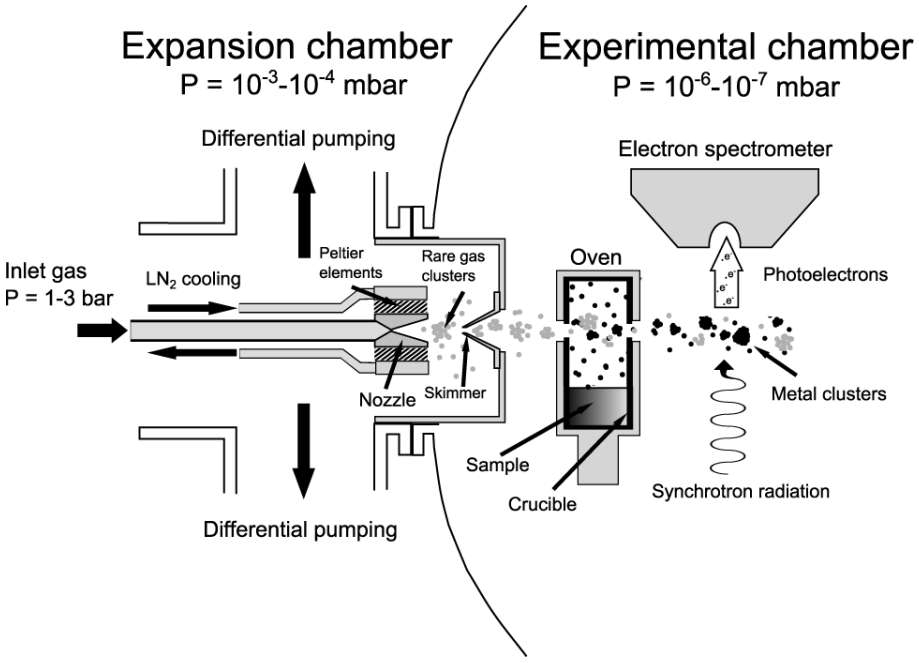

Figure 2.4. Schematics of the pick-up source. Figure provided by M.-H. Mikkelä.

the crucible there are two oppositely placed circular 3 mm diameter openings through which the argon-cluster beam can enter and the resulting metal-cluster beam can exit. The crucible is placed inside a heating arrangement which is either resistive or inductive. For the work presented in this thesis, resistive heating has been used to vaporize lead (paper V), while the inductive heating setup has been used in the tin cluster experiments (paper II), as the latter requires higher temperatures. The induction arrangement consists of a water-cooled copper induction coil which surrounds the crucible. The heating is achieved by the resistive losses of the eddy currents induced in the conductive molybdenum crucible. In the case of resistive heating, current is sent through a tantalum wire insulated by boron nitride and the sample is heated though absorption of the thermal radiation from the wire.

The experimental method (photoelectron spectroscopy) applied in the present work and described in detail in the next chapter is demanding in the sense of sample density. Thus, the implemented cluster sources have been used in the regimes when the densities of the cluster beams have been the highest. The principle of operation for both sources is such that an increase in the cluster beam density simultaneously means an increase in cluster size. For the gas-aggregation source the densest beam has been achieved when the clusters contained from ~10^3 atoms and above. The pick-up source generally produces smaller clusters, from a few tens up to a few hundreds of atoms, where the efficiency of our gas-aggregation source is worse. This is why the EXMEC pick-up source has been developed and implemented. In compari-

son with the oven-based gas aggregation source the EXMEC setup can reach much higher temperatures for vaporization of the samples. The heating arrangement of the pick-up source allows temperatures well above 1000 degrees Celsius while the oven-based gas-aggregation source is limited to a few hundred °C. Thus, the EXMEC source allows production of clusters in an important size-range, unreachable for the gas-aggregation source in our experiments, and can also vaporize high-melting point metals for which the oven of our gas-aggregation source is insufficient. However, to produce large (~10^3 atoms and above) clusters out of these high melting point materials, one can turn to the sputtering-based gas-aggregation source. For the case of nanoalloy clusters we have, for both cases presented here (NaK and CuAg), used the gas-aggregation source. There have been several reasons for this, both fundamental and technical. The gas-aggregation source allows creating nanoparticles close in size to the practically interesting range, where the laws known from the macroscopic world can be studied at the nanoscale. Additionally, it is easier to control the mixing ratio of two vapours with a magnetron source. Also, the metal cluster signal from the chosen systems is obscured to a larger extent by the photoelectron signal from argon in the pick-up source. A future perspective is to combine the gas-aggregation and the pick-up source: to seed the metal vapour created in the EXMEC oven by a beam of metal clusters instead of the argon cluster beam and in this way promote formation of clusters with a certain core-shell geometry.

3. Photoelectron spectroscopy applied to clusters

The work presented in this thesis has been aimed at probing the electronic structure of free metal clusters using synchrotron radiation. Here an overview of the probing method is given in the first section, followed by descriptions of the experimental equipment, the expected spectral response and finally, the details of the spectral analysis.

3.1. Photoelectron spectroscopy

Photoelectron spectroscopy is based on the photoelectric effect, i.e. the emission of an electron from an object, e.g. atom, cluster or solid, due to absorption of a photon of sufficient energy. The probing radiation can be generated by different sources, e.g. a laser, a discharge lamp, or, like in the experiments in this work, at a synchrotron facility (see section 3.2.1). If the energy of the absorbed photon is high enough, an electron from the sample can be emitted with the kinetic energy, E_{kin}, given by the photoelectric equation

$$E_{kin} = h\nu - \left(E_f - E_i\right) = h\nu - E_{bin} \qquad (3.1)$$

where $h\nu$ is the photon energy, E_f and E_i are the final and initial state energies of the system, and $E_{bin} = E_f - F_i$ is the electron binding energy. The kinetic energies of the emitted photoelectrons can be determined by an

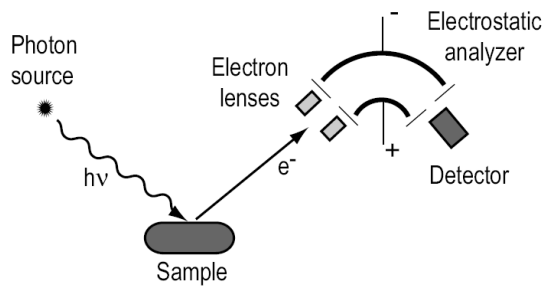

Figure 3.1. The principle of photoelectron spectroscopy. Figure provided by S. Peredkov.

electron-energy analyser (electron spectrometer) [17], and their binding energies can be derived, provided that the photon energy is known. In many cases, for the studies of valence levels/bands, ultraviolet photon energies are enough while the ionization of the deeper-lying core levels requires x-ray photons. Depending on what kind of radiation is used, photoelectron spectroscopy is referred to as either UPS (Ultraviolet Photoelectron Spectroscopy) or XPS (X-ray Electron Spectroscopy). The principle of PES is shown in figure 3.1.

The x-rays used in the present experiments (see details below) are able to reach a few μm into a condensed matter system. Thus not only the outermost atomic layer of the sample can be ionized but also its inner part—the bulk. The photoelectrons emitted by the bulk atoms undergo efficient attenuation due to the interaction with the atoms and electrons of the system. This attenuation can phenomenologically be described via an exponential dependence, $e^{-x/\lambda}$, where x is the distance the photoelectron must travel to reach the surface and λ is the inelastic mean free path, i.e. the average distance the photoelectron travels between consecutive inelastic scattering events. This mean free path, or escape depth, of electrons in solids is dependent on the electron energy: it has a minimum at some tens of eV and increases both with increasing and decreasing electron energy. If the photon energy is chosen so that the ejected electrons have energies near the minimum, then a high surface sensitivity, i.e. the most intense response from the surface relative to the bulk signal, will be achieved. On the contrary, if one instead chooses to use a very high photon energy or a photon energy just above the ionization threshold, the resulting long mean free paths will provide a more favourable situation for the photoelectrons coming from the interior of the sample.

When choosing photon energy one has to take into account the photon energy dependence of the surface-to-bulk intensity ratio but also the spectral photon flux provided by the radiation source and the ionization cross-section for the level under investigation. The cross-section can be a non-monotonous function of the photon energy with maxima and minima [18]. Additionally, one must consider the achievable radiation bandwidth which can be varying for different photon energies and thus influencing the total energy resolution in an experiment.

3.2. Practical setup

For the photoelectron spectroscopy experiments presented in this thesis, photoelectron emission has been studied using synchrotron radiation as a probing tool. The experiments have been performed at the MAX-lab synchrotron radiation facility (figure 3.2). In section 3.2.1, the generation of synchrotron light and the way a specific photon energy is selected in the present experiments is described. As mentioned above, the photoelectron energy is measured using an electron energy analyser described in section 3.2.2.

3.2.1. Light source—synchrotron radiation

Synchrotron radiation is emitted when charged particles, e.g. electrons, are accelerated. For relativistic electrons, the radiation is emitted in a narrow cone in the forward direction. Relativistic electrons can be produced and stored in stable orbits in storage rings using magnetic fields. Storage rings usually consist of a number of straight sections with so-called bending magnets in the junctions between them. At earlier synchrotron facilities the radiation generated in these bending magnets was the main tool used for various types of experiments, e.g. photoelectron spectroscopy. The MAX II storage ring, which acted as light source in the experiments of this work, is a so-called 3rd generation synchrotron radiation source. In such a source, the bending magnets used to maintain the beam in its orbit are not the main sources of the output light. Instead, large arrays of alternating dipole magnets, wigglers and undulators, are placed in the straight sections of the storage rings. These so-called insertion devices cause the electrons passing between the magnets to move in an oscillatory trajectory, emitting radiation

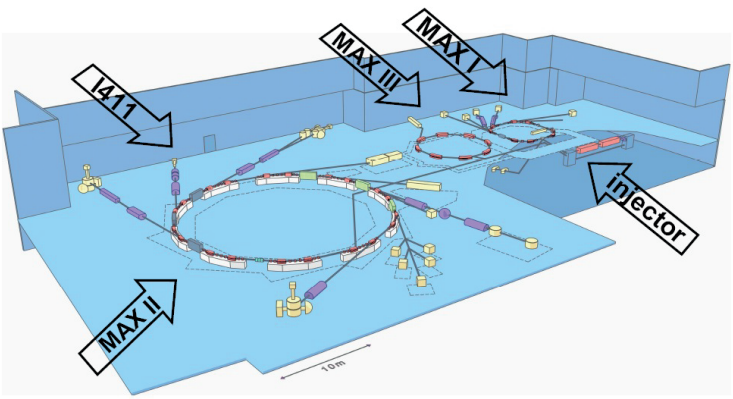

Figure 3.2. The MAX-lab synchrotron radiation facility. Figure provided by S. Peredkov and MAX-lab.

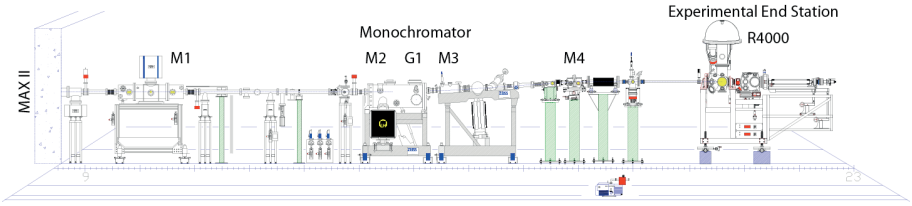

Figure 3.3. The I411 soft x-ray undulator beamline. Figure provided by M. Lundwall.

mainly along the insertion device axis. For undulators, one of which was used in this work, the dipole magnets of the array are arranged in such a way that the radiation interference is constructive for one specific wavelength. In this way, a high peak intensity can be achieved for this wavelength while the others are damped. The wavelength to be amplified can be changed by varying the strength of the magnetic field. Thus produced synchrotron radiation has a number of properties making it especially suitable for spectroscopic purposes. Output light of any wavelength in a continuous interval between the infrared and hard x-rays can in principle be achieved (although not by one and the same undulator). It has a very high brilliance, is well collimated and also has a well-defined time structure.

The experiments in this work were carried out at the undulator beamline I411 (layout in figure 3.3) at the MAX-II storage ring. The undulator for this beamline produces synchrotron radiation in an energy interval of ~40-1500 eV. Before the light is used in an experiment it is monochromatized. This is done using a modified Zeiss SX700 monochromator that disperses the light and makes it possible to select a narrow wavelength interval. The light from the undulator is reflected onto the first mirror of the monochromator by another, spherical, mirror (M1). The first part of the monochromator is a plane mirror (M2) that reflects the incoming light onto a plane diffraction grating (G1) with 1221 lines/mm where light of different wavelengths is reflected at different angles. Then the light is focused onto an adjustable (0-800 μm) exit slit by a plane elliptical mirror (M3). The desired wavelength is selected by tilting both the grating and the plane (M2) mirror simultaneously according to a certain algorithm, which allows a fixed focus position. Having exited the monochromator the radiation is refocused, both vertically and horizontally, by a toroidal mirror (M4), into a certain point in the end station, where the electron spectrometer also has its focal point and where the sample is placed.

3.2.2. Electron spectrometer

The kinetic energies of the ejected photoelectrons are measured using a hemispherical Scienta R4000 electron analyzer/spectrometer (schematics in figure 3.4). The incoming electrons are focused by an electrostatic lens and then forced to travel in a radial electric field between two hemispherical

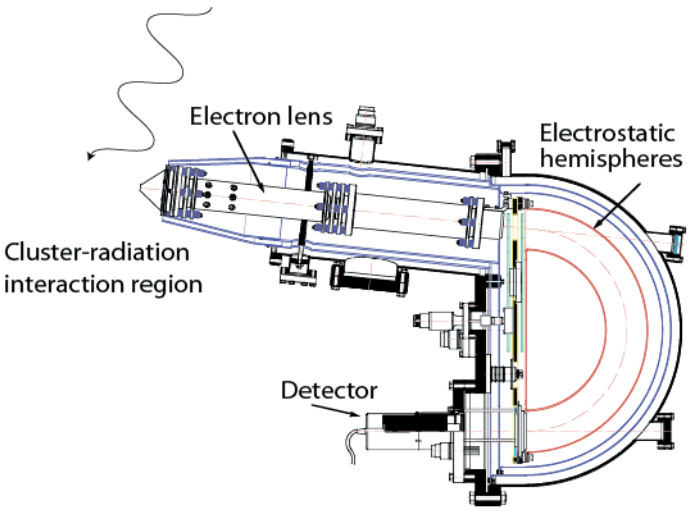

Figure 3.4. Schematics of an electron analyser. Figure provided by M. Lundwall.

electrodes. Electrons of different kinetic energies have their trajectories differently bent and only electrons within a specific energy interval can reach the detector system. The width of this interval is chosen by varying the electric potentials of the lens and the hemispherical electrodes. As the detector has a fixed number of physical channels, a wider detection interval leads to a lower energy resolution. The result of a measurement with such a spectrometer is a so-called photoelectron spectrum: a distribution of the electron signal over a kinetic/binding energy interval. The signals from the electrons arriving at each detector channel (corresponding to a certain energy interval) within a chosen time are summed up and these intensities for all detector channels constitute the spectrum.

3.3. Spectral response

3.3.1. Free atoms

When photoelectron spectroscopy is used to probe the electronic structure of single atoms, ionization-transition selection rules and the spin-orbit splitting give rise to a number of peaks in the photoelectron spectrum. For example, a rare gas atom in its ground state has only filled shells. If ionized, the atom is left in one of the allowed spin-orbit split states given by the coupling between the angular momentum, l, of the level from which the atom is removed, and the electron spin, s, which is either plus or minus ½. According to the spin-orbit coupling rules, there are, except for $l = 0$ (s-states) then two possible spin-orbit split states for the ionized atom, so ionization of any level

with $l > 0$ gives rise to two peaks in the spectrum. s-state ionization gives only one peak.

If there are open shells in the ground state of the atom, the situation is different. In alkali metal (e.g. sodium and potassium) atoms, the valence level is a half-filled s-shell (one electron). The core-levels are fully filled. If a core level in such an atom is ionized, the appearing vacancy in this level will couple to the valence electron which opens up several possible spin-orbit split states for the ionized atom. The core level from which the electron is removed has, provided it has $l > 0$, two possible electronic configurations, giving rise to a total of four possible spin-orbit states for the atom. For example, the electron configuration for a potassium atom is $1s^2 2s^2 2p^6 3s^2 3p^6 4s$. If the 3p core level is ionized, the angular momenta of the 3p level $(l = 1)$ and the 4s valence level $(l = 0)$ will couple to a total momentum, $L = 1$. Likewise, the spins will couple to a total spin, $S = 0$ or 1. This will give two terms, one singlet and one triplet and hence four spin-orbit split states, which correspond to four peaks in the photoelectron spectrum. This scheme of LS-coupling is known to be relevant for lighter elements. With increasing mass however, the case of jj-coupling becomes more and more prominent. In this case, the orbital- and spin-momenta of each electronic shell first couples into a total momentum j for the shell. The j-momenta of the individual shells then couple to each other and the result is two doublets. The total number of states is four also in this case. The transformation from the LS- to jj-coupling can be well seen, for example, in the ionization of the d levels in separate atoms of copper and silver. While in the case of copper 3d ionization there is a singlet and a triplet, in silver 4d the lines are grouped in two doublets [9].

Even in the simplest case of photoemission from a separate atom, each spectral feature in the observed signal assumes a certain spectral profile. Again, in the simplest case, the profile is a symmetric peak with a maximum corresponding to the most probable binding energy. The observed width of the peak is determined by many different mechanisms, defined both by the inherent properties of the investigated system and by the experimental conditions.

Core-level photoemission leaves the ionized atom in an excited state. This state will decay after a finite time, the lifetime of the excited state. For the core levels of lighter elements this most often proceeds via Auger decay, when an electron from a higher shell will fill the core vacancy and another electron will be emitted. This leaves the system in a doubly ionized, relaxed state.

If no external broadening mechanisms were present, the lifetime broadening would give a peak of a Lorentzian shape. In practice, however, the peaks are always further broadened due to the experimental conditions. Among the most important broadening reasons for the present work are the limitations in photon monochromaticity and photoelectron detector energy resolution. The

broadening contributions due to these mechanisms are described by a Gaussian shape. There are also other contributions to the line broadening. In the general case for free atoms, collisions between them can broaden the Lorentzian while the Gaussian will have its width further increased by the Doppler effect due to the thermal energy of the system. The Gaussian width, ΔE, could be estimated in a photoelectron spectroscopy experiment as

$$\Delta E = \sqrt{\Delta E_m^2 + \Delta E_{sp}^2 + \Delta E_{th}^2} \qquad (3.2)$$

where ΔE_m is the width introduced by the final spectral interval of the incident radiation cut out by the monochromator slit, ΔE_{sp} is the width due to the limited spectrometer resolution and ΔE_{th} is the width due to thermal broadening. The contributions from the experimental equipment are known, while for the inherent spectral line width of an atom this is not always the case. The result of the Lorentzian and Gaussian contributions to a spectral line-shape is the so-called Voigt profile (a convolution of a Lorentzian and a Gaussian) which adequately describes the peak.

Apart from the main spectral lines due to the direct ionization of a certain energy level discussed above, various other features due to the same primary ionization process can be present in the spectra. Some of them are referred to as satellite features and arise from numerous processes, e.g. photoelectron energy-losses to excitations of valence electrons to higher, normally unoccupied states. The kinetic energy loss in these "shake-up" processes causes the photoelectron signal to appear at a higher binding energy in the spectrum. Excitation to several levels leads to a certain set of discrete features on the binding energy scale [19].

The considerations presented above are in general valid not only for the core-level ionization case, but also for the valence ionization. The multiplet structure of the spectrum is then caused by different possible configurations of the final ionic states with an electron vacancy in the valence shell. One of the main differences for the valence state ionization in separate atoms is the infinite lifetime of the ionized states, since no de-excitation occurs after the ionization. This leads to practically zero Lorentzian widths, so the spectral shape of such valence lines is purely Gaussian.

3.3.2. Solids

As a rule, the spectral response of solids differs significantly from that of the corresponding free atoms. As discussed in the introduction, the discrete valence levels of the atom are replaced by continuous valence bands in the solid. Due to the wide range of electron energies of these bands, the valence photoelectron spectra no longer consist of individual discrete peaks due to the different possible ionic states but rather wide features extending over

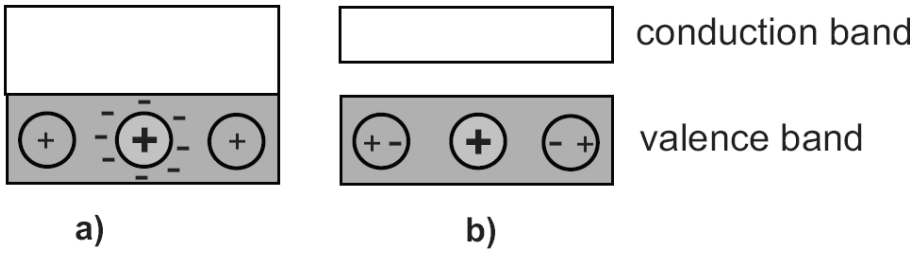

Figure 3.5. a) Complete metallic screening. b) Incomplete polarization screening. Figure provided by S. Peredkov.

several eV on the binding energy scale, reflecting the distribution of the electronic density of states in the valence bands.

Also for the core levels the situation is different. Since the core orbitals remain localized they, as a rule, show up as relatively narrow, atomic-like peaks also in photoelectron spectra of solids. The number of multiplet ionic final states, however, is generally not the same as for the corresponding separate atoms. Core-level solid-state spectra can display splittings of other origins. These splittings can be due to differences in both initial- and final-state energies of the probed atoms in the sample. One of the peculiarities of the core-level spectra is the often well-separated response of the surface atomic layer and of the bulk. The initial and final state energy can vary for the surface and bulk atoms due to the lower coordination number at the surface (the coordination number can also vary between different surface sites). For the initial states this can result in a significant difference in the cohesive energy for the atoms of these sites. This can cause each electronic state to give rise to one peak for each site in the core-level photoelectron spectra, often one for the surface atoms and one for the atoms in the bulk. The differences in the final-state appear due to differences in the screening efficiency. For metals, this is not relevant as the free mobility of the valence electrons always provides a complete screening of the core-hole (figure 3.5 a), regardless of whether it is positioned at the surface or in the bulk. For insulators and semiconductors, the situation is different. As the valence electrons are not allowed to move freely throughout the sample, the complete screening present in metals is not possible. Instead, the core-hole will polarize the neighbour atoms, attracting the electrons (figure 3.5 b). This partial, polarization screening will, typically, be less efficient with fewer neighbours so the decrease in energy will be smaller for surface atoms than for atoms in the bulk.

Returning to the example of potassium discussed above for the atomic case, one observes that the spectral response for the solid state changes in the way described in the two last paragraphs for the general case. If the 3p core level is ionized in a solid, the spectrum can be well-explained under the assumption that there is no coupling between the 3p-level electrons and the electrons of the valence-band [20]. In such a case the total angular momen-

tum of the ionic state would be the same as the angular momentum of the 3p level, $l = 1$. Because of the two possibilities for the spin $\pm ½$, there would be two spin-orbit split states. Each of these states gives rise to two peaks, one for the bulk atoms and one for the surface atoms, as discussed above. As will be discussed in detail below, the photoelectron spectra of alkali- and alkali-earth metal clusters created by the gas-aggregation source resemble to a great extent in the energy and spectral shape those of the corresponding solid metals, both in the valence and in the core-level response.

There are also differences between the atomic and solid cases regarding the peak shapes. The shake-up processes existing in the free-atom case are present also in solids, but as the available states to which the electrons can be excited are no longer discrete, neither are the satellites. In metals the shake-ups manifest themselves in the spectral shape of the photoelectron main features. Valence-band electrons are excited into the conduction band by the outgoing photoelectrons which leads to corresponding kinetic energy losses for the latter. The excitation probability decreases with energy above the Fermi edge, which results in asymmetric tails of the main features towards higher binding energies. To account for this process, the Voigt profiles of the atomic case are replaced by so-called Doniach-Šunjić profiles [21], featuring an asymmetry parameter, the singularity index, α. The spectral profiles are thermally broadened also in solids, but the cause for this broadening is here vibrations in the lattice. The total Gaussian width, due to this broadening and due to the instrumental contributions, can still be estimated by formula (3.2), even if the thermal broadening term now doesn't have exactly the same origin. For the metallic clusters studied in the present work the spectral shapes of the core-level features have also been assumed to have Doniach-Šunjić profiles.

In photoelectron spectra of solids there are satellites without any correspondence in the atomic case. Among these are the plasmons. These are quantized collective oscillations of the valence electrons relative to the ion lattice, predicted already in the simplest theoretical description of metallic solids, the Drude free electron model [22], which is known to be a satisfactory good approximation for the alkali metals. Plasmons can be excited directly by the interaction between the electron gas and the created core hole, and are then called intrinsic, or by scattering of the outgoing photoelectrons on the electron gas as a whole, and are then referred to as extrinsic plasmons. Both types of plasmons have the same excitation energy [23]. According to the Drude model the bulk plasmon energy, E_{bp}, is given by

$$E_{bp} = eh\sqrt{\frac{n}{\pi m_e}} \qquad (3.3)$$

where m_e is the electron mass and n is the electron density. The surface plasmon energy, E_{sp}, is then, in the planar macroscopic case, given by $E_{sp} = E_{bp} / \sqrt{2}$. Plasmons have been observed in numerous photoelectron spectroscopy experiments on planar macroscopic solids, see e.g. [23-25] for Na, K, Mg and Al, the elements for which plasmon excitation in clusters have been investigated in this thesis. In photoelectron spectra, the plasmons show up as features centred at binding energies an integer number of plasmon energies higher than the main feature. In the case of a single-plasmon excitation there should, in principle, be one plasmon peak for each peak in the main feature, both surface and bulk ones, though in our treatment we assume that the photoelectrons from the surface are less likely to excite the bulk plasmons. In practice however, all of these peaks can not always be resolved. Instead, one has to treat several close-lying peaks together as one peak. In photoelectron spectra plasmon-related satellites have been observed also separated from the main features by energies corresponding to more than one quantum of plasmon excitation. These features have been interpreted as due to harmonic plasmon overtones [23, 25]. As will be discussed in detail below, for the free nanoscale metallic clusters created in the present work, both single- and double-quantum plasmon excitations have been observed in the experiments.

For solids, the photoelectron spectra have a non-uniform and often structureless background of significant intensity. This background appears due to multiple scattering mechanisms present in solids but absent for free atoms and molecules. Photoelectrons and Auger electrons can lose energy to excitations of electrons to higher states (like those in metals described above, or excitons in non-conductive substances), phonons, plasmons, and secondary ionization processes etc. These secondary electrons are also recorded after they leave the system, contributing to the background of a spectrum. The backgrounds are difficult to analyse and describe as a whole for a long energy interval. To circumvent this problem one can split the energy range under investigation into several shorter parts containing the relevant features and fit them separately.

3.3.3. Clusters

As mentioned earlier, for clusters, the spectral response depends on the cluster size. In this work, most of the produced clusters are large enough to be considered metallic. Hence, they can be expected to display solid-like features in the recorded photoelectron spectra. Due to the remaining charge on the initially neutral cluster after the photoionization, as opposed to the grounded solid, there is an additional electrostatic interaction between the cluster and the outgoing electron that increases the ionization energy for such initially neutral clusters. The binding energy is also influenced by the

curvature of the non-planar cluster surface. As the clusters become larger the combined effect becomes weaker and the ionization energy gradually approaches the solid value [26]. The core levels of large, initially neutral, metal clusters show up in photoelectron spectra as solid-like features shifted towards higher binding energies relative to the solid case. As briefly mentioned above, also the shape and width of the cluster spectral features have been shown to resemble those of the corresponding solids to a large extent. In the experiments of this work, the nature of the broadening contributions is considered the same as for solids, and Doniach-Šunjić profiles are used for fitting the peaks. There should also be an additional broadening due to the size distribution of the produced clusters which becomes increasingly important with decreasing size.

The spectral shape of the valence band response in a photoelectron spectrum reflects first of all the density of states which varies with size—as more and more atoms are added new states are introduced until a solid-state-like electronic structure is reached. For this work the size dependence of the valence band on-set, i.e. the lowest binding energy of the valence electrons, as well as the width of the band, are the most relevant. With increasing cluster size the valence band width increases and the on-set shifts towards the solid-state limit.

In the present experiments, the cluster size can be estimated from the binding energies of electrons, ejected either from the core or valence levels. As mentioned above the binding energies of both the core and valence electrons should shift away from the solid state values with decreasing size. Provided that the clusters are large enough to be considered metallic, which they are in most cases in this work, they can be approximated as uniform, conducting spheres [26]. The cluster radius, R, can then be estimated from the equation

$$E_{cluster}^{Z} = E_{solid}^{Fermi} + \phi + \frac{Z + ½}{4\pi\varepsilon_0} \cdot \frac{e^2}{R} \qquad (3.4)$$

where $E_{cluster}^{Z}$ is the binding energy of a cluster of initial charge Z, E_{solid}^{Fermi} is the solid state binding energy relative to the Fermi level (which is the binding energy usually determined in solid state experiments) and ϕ is the solid state work function. Assuming that the cluster atomic density is the same as for the macroscopic solid, the number of constituent atoms, N, can then be calculated through

$$N = \frac{\rho}{m} \frac{4\pi R^3}{3} \qquad (3.5)$$

where ρ is the solid state density and m is the atomic mass. The presence of a size distribution in the cluster beam makes the situation more complex: electrons with a range of binding energies contribute to the experimental signal. The advantage of the core-level spectra for determining the cluster size is in the well-defined shape and maximum of a typical core-level response. The maximum of such a core-level response corresponds to the most abundant size in the distribution, and the radius calculated from this maximum energy and number of atoms will be close to the mean value of the produced size distribution. In a corresponding estimation of the cluster radius from the on-set of the valence band, the presence of a size distribution and the DOS-defined shape leads to larger uncertainties: The energy value for formula 3.4 above is determined from a *flank* of the valence band feature, and not at the maximum of the signal which gives an estimate shifted either towards larger sizes, for initially neutral clusters or cluster cations, or towards smaller clusters, for initially negatively charged clusters.

As for the presence of satellites in the cluster spectra, the same features as found for the solid-state case can be expected, and have indeed been observed. Concerning plasmons in clusters (which is the topic of papers III and IV) however, clear differences to the solid state case have been observed in experiments performed with other probing methods than photoelectron spectroscopy. In free clusters, the most common approach to the studies of plasmons has been optical absorption cross-section measurements which give the value of the so-called Mie resonance [27]. The implementation of this technique to bulk plasmons is problematic both theoretically and experimentally [22, 28]. The Mie absorption resonance, which is known to exist for small metallic spheres [29], is the surface plasmon mode for metallic particles which are considerably smaller than the wavelength of the absorbed radiation. The excitation energy of the Mie plasmon has a limit value $\sqrt{3}$ times smaller than the solid state bulk plasmon value. Photoelectron spectroscopy experiments performed earlier by our group have not shown any presence of Mie-energy plasmons for nanoscale K clusters. The derived surface plasmon excitation energies have instead been found to be rather close to those of planar solid surface plasmons [30]. Regarding the excitation of plasmon overtones in clusters, the laser-excitation-based methods have again only been used to probe the surface plasmons. A change in the fragmentation pattern of Na clusters following multi-photon absorption has been interpreted as due to harmonic excitation, or overtone excitation as it is called [31].

3.4. Data analysis

The core-level photoelectron spectra were analysed using an Igor Pro-based script by Edwin Kukk [32]. In this program, the lines can be given certain pre-defined shapes such as e.g. Voigt or Doniach-Šunjić profiles. For each line, certain initial values of binding energies, intensities, widths of Lorentzian and Gaussian contributions to spectral profiles, and asymmetry factors can be given independently. The line parameters (intensity, width, position) can be fixed, or linked, to those of the others. If the spin-orbit and bulk-surface splittings are known, the energy difference between the peaks can be fixed to the relevant values. Likewise, for intensities, the known spin-orbit ratios can also be fixed. Further, the singularity indices and the widths of Lorentzians and Gaussians can be fixed if the values are known, or linked to those of other lines if the relations are known. Also, different types of backgrounds can be used but for the work in this thesis the backgrounds have always been approximated as straight lines. The experimental features are fitted using the least-squares method.

4. Results & Discussion

4.1. Surface segregation in self-assembled nanoalloy clusters: Papers I & VI

When a condensed matter system is created out of separate atoms or molecules, it strives to have its constituent atoms arranged in such a way that the total energy is minimized. This is valid also for metals, the type of materials studied in the present work. For clusters consisting of just one type of atoms this is a question of geometric structures and interatomic distances. When atoms of different elements are mixed, like in an alloy, there is also the issue how these atoms arrange themselves relative to each other.

When a cluster is formed from vapours of elements A and B the parameters most relevant for the resulting spatial distribution of the atoms are the bond strengths A-A, B-B and A-B. An A-B bond that is strong compared to the other bonds will typically lead to a well-mixed cluster, while a comparably weak A-B bond instead will promote segregation. A quite common situation for a bi-component alloy is when one of the substances has a weaker bond between its own atoms (A-A or B-B) than the other substance, and as a result is pushed out to the surface. An atom at the surface has fewer nearest neighbours, or in other words, a lower coordination number than a bulk atom. The total energy release per atom, roughly proportional to the number of the bonds with the neighbours, is smaller for the surface atoms than for the bulk ones. Placing the species with the weaker bond at the surface thus leads to a smaller increase of the total energy of the system. The energy per bond of the elemental solid can be estimated by dividing its cohesive energy by the coordination number of its solid. If the systems are alike, i.e. if they have the same crystal structure, like for example two alkali or two coinage metals as in the present study, or two inert gases, like in the previous works of our group, one can compare the cohesive energies directly. The principle of energy minimization favours the element with the higher cohesive energy to be placed in the bulk. Apart from the bond strengths also the size of the atoms matters, with the larger of the two species being more likely to be found at the surface. Also, parameters like temperature, pressure and time in the cluster formation process are important. Surface segregation in free clusters self-assembled out of two different elements of the same type has been observed earlier for noble gas clusters [33-35], manifested in a way similar to the expectations described above.

In the work presented here we have, using the gas aggregation source, produced free NaK (paper I) and CuAg (paper VI) clusters from the mixed vapours of the two metals in question. The electronic and geometric structures of these nanoalloy clusters have been investigated utilizing photoelectron spectroscopy. With the discussion in the previous paragraph in mind, and noting that the cohesive energy is higher for sodium than for potassium and that K atoms are larger than Na atoms, it is reasonable to expect a potassium-dominated surface for mixed NaK clusters. Likewise, concerning the CuAg nanoparticles, one can expect a surface consisting mainly of silver.

In the case of sodium-potassium clusters the resistive oven has been used as a vapour source. In an initial series of experiments we have produced pure, mono-component Na and K clusters (with one sample at a time placed in the oven) and probed their core-levels for which the surface and bulk responses are known to be resolved (2p for Na, 3p for K). The corresponding spectra are presented at the top of figure 4.1 below. In the next series of experiments we have simultaneously placed approximately equal volumes of sodium and potassium (~1:2 in mass) into the oven and recorded spectra of

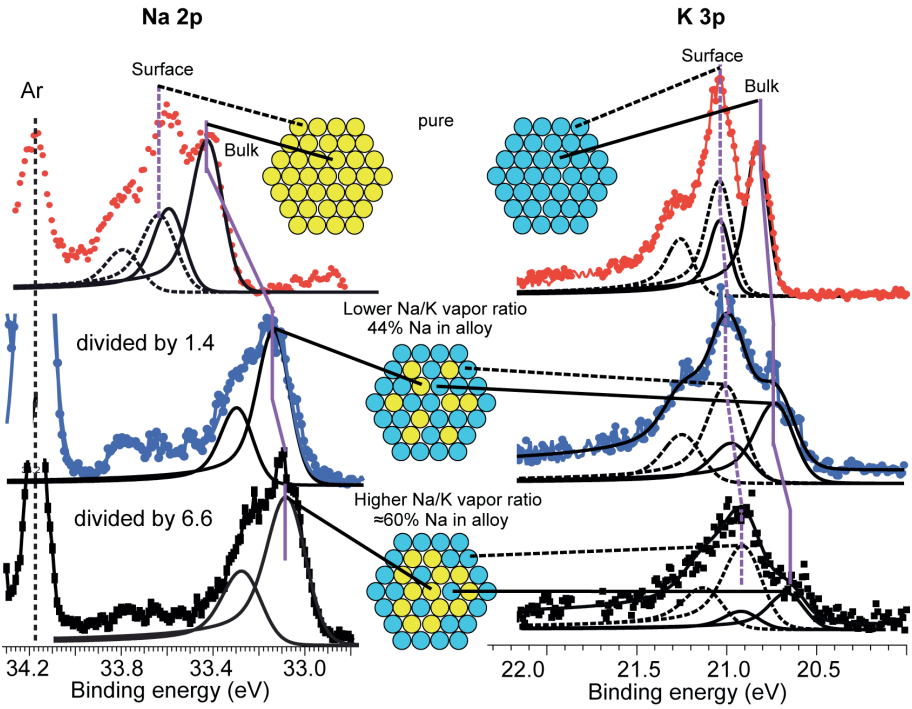

Figure 4.1. Photoelectron spectra of the Na (2p) and K (3p) core levels. The top spectra are recorded for pure clusters while the others are recorded for mixed clusters formed from different Na/K vapour ratios (middle: lower, bottom: higher). In the mixed-cluster cases the Na and K signals are parts of the same spectra, where the Na intensity has been divided by 1.4 (middle) and 6.6 (bottom). Absolute calibration has been done using Ar lines. The binding energies are relative to the vacuum level.

the clusters formed out of the vapour mixture—in the energy range containing both the Na 2p and K 3p responses. As potassium produces a considerably higher vapour concentration than sodium at the same temperature, there has for a certain time been a surplus of this element in the primary vapour mixture. At a later time of the measurement however, as K was to a large extent used out, we instead have had a situation with a surplus of sodium. This allowed us to study clusters formed from two different Na/K vapour-concentration ratios, one lower (middle spectra in figure 4.1) and one higher (bottom spectra).

If we first look at the pure-case spectra, we see that their shapes are practically identical to those of the macroscopic metal samples and both cases (Na and K) can be fitted with four peaks, bulk and surface components of each of two spin-orbit states, $2p_{3/2}$ and $2p_{1/2}$ for Na and $3p_{3/2}$ and $3p_{1/2}$ for K. For the clusters produced from mixed vapours the situation is clearly different. For K 3p, one can note that the spectra are shifted towards lower binding energies compared to the pure case. If the probed clusters were pure then such a shift would correspond to an increase in size. However, we also see that the K 3p bulk intensity has decreased relative to that of the surface. For pure clusters this would imply a decrease in cluster size. This contradiction—between the lower binding energy and the decrease in the relative response of the bulk—suggests that the clusters are not pure but mixed. Switching to sodium one can see that, apart from the negative binding energy shift, which is clearly larger than for K, only one pair of peaks is required to fit the Na spectrum. This can be either the bulk or the surface pair of the two spin-orbit states. The decrease in the K 3p relative bulk intensity mentioned above suggests that what we see are the spectra of clusters consisting of a mixed NaK bulk and a strongly K-dominated surface. This structure explains the larger binding energy shift for the Na spectra. With a potassium-dominated surface the cluster work function would be that of K, i.e. for the photoelectrons originating from K atoms the work function is the same as in the pure case, while for electrons coming from Na atoms it is about 0.5 eV lower. For the K 3p level, the smaller shift compared to the pure case (relative to the macroscopic sample response) is a result of differences in the local chemical environment in the alloy and probably also in size. These differences of course also matter for the Na 2p shift.

The size of the produced clusters can be estimated from the relative intensity of the bulk and surface peaks. This relative intensity reflects the size-dependent ratio between bulk and surface atoms. For the bi-component case one has to take into account the difference in the ionization cross-section for Na 2p and K 3p and the mean free path between the elemental solids (the latter happens to be approximately the same at the relevant photon energy). From comparisons with previously published measurements on pure Na and K clusters [30, 36], the clusters are estimated to contain 10^3-10^5 atoms.

From the different peak intensities it is also possible to extract information about the bulk stoichiometry of the clusters, i.e. how large are the fractions of Na and K. Assuming a homogeneous mixture in the bulk, and again taking into account the different ionization cross-sections, we find that in the lower Na/K vapour-ratio case (middle spectra) the bulk consists of ~40% Na while in the higher Na/K vapour ratio case (bottom spectra) the Na constitutes ~60% of the bulk. This suggests that even when sodium is the majority species in the clusters, potassium still strongly dominates the surface.

The outcome of our experiments on CuAg clusters is similar. Also in this case the gas-aggregation source has been used but instead of the oven, the sputtering source has been implemented to vaporize two targets, one consisting of ~60% silver and ~40% copper, the other one vice versa. Considering the volumes sputtered from the target and the molar volumes of the elements in the two cases, the ratios of copper-to-silver atoms should be approximately 1:1 and 2:1, respectively. Photoelectron spectra have been recorded in the binding energy range 3-17 eV, where the 3d and 4s levels of copper as well as the 4d and 5s levels of silver can be found (the response from the s-levels is however rather weak at certain photon energies within these measurements). The binding energy region has been probed with several different photon energies from 40 eV (cross-section maxima for both elements) up to 108 eV. As the silver signal weakens to a much greater extent with the photon energy increase over this interval, due to a rapid fall of the Ag 4d ionization cross-section, the spectrum with the highest energy will strongly favour the copper response, which allows us to disentangle the two overlapping signals from Cu 3d and Ag 4d. A set of spectra is presented in figure 4.2, together with a spectrum of pure silver clusters ($h\nu$=40 eV, at the top) and one of pure copper clusters ($h\nu$=108 eV, at the bottom) for comparison. Starting from the bottom one can note that the Cu 3d band is shifted upwards by ~0.5 eV for the alloy clusters compared to the pure copper clusters and also that the band width is considerably narrower. Our interpretation of this narrowing is that copper atoms can be either only in the bulk or only at the surface. With no correspondingly strong change in the silver signal, it is likely that this latter element is present both in the bulk and at the surface. Considering that silver atoms are significantly larger than copper atoms and that the cohesive energy is larger for Cu than for Ag, the most probable explanation for the Cu and Ag spectral behaviour is that the cluster surface is made up mostly of silver while the bulk consists of both elements. This is what we see also for the case when the target made up of 60% copper was sputtered.

In figure 4.3, three spectra of clusters of different stoichiometry, formed out of vapour mixtures with ~1/3 silver atoms, ~1/2 silver atoms and pure silver, respectively, are presented. Here one can notice a clear decrease in silver spin-orbit splitting with the decreasing fraction of silver atoms. Such a

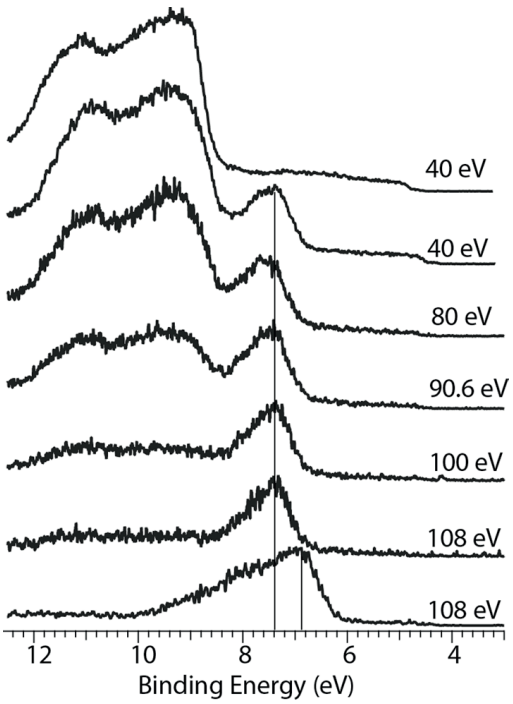

Figure 4.2. Photoelectron spectra of CuAg-clusters with approximately equal amounts of silver and copper atoms in the primary vapour mixture, recorded at different photon energies. For comparison, also spectra of pure silver clusters (top spectrum) and pure copper clusters (bottom) are included. Absolute calibration has been done using Ar lines. The binding energies are relative to the vacuum level.

change has been seen earlier in studies of concentration dependence in silver alloys, and has been attributed to differences in silver-silver coordination [37]. When the copper-to-silver ratio increases, the silver atoms will more likely have copper-atom neighbours, which changes the local electric field and decreases the spin-orbit splitting [37]. This suggests that the constituent elements in the bulk of our alloy cluster are well intermixed.

These findings on the geometric structure of self-assembled, bi-component, nanoalloy clusters, together with previous results from our group on clusters formed from noble-gas mixtures [33-35], provide a consistent picture on how the constituent elements arrange themselves relative to each other at the nanoscale, in the absence of any substrate influence. The element with larger atoms and lower cohesive energy is generally more likely to be found on the surface, than the element with smaller atoms and higher cohesive energy. The studies of free non-supported nanoalloy clusters are especially important as a test for fundamental theory predictions [38]. NaK alloy clusters have been a good model system in this respect. Our more recent work on CuAg nanoalloy perhaps in addition has a more practical side. Silver nanoparticles have been used for quite some now as catalysts for

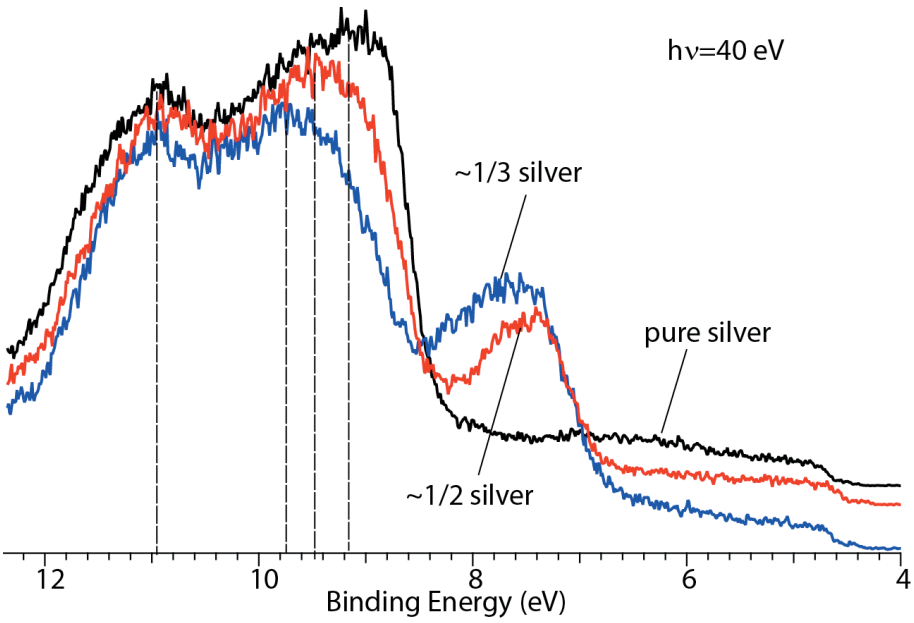

Figure 4.3. Photoelectron spectra of clusters consisting of ~1/3 silver atoms (blue spectrum), ~1/2 silver atoms (red) and only silver atoms (black). Absolute calibration has been done using Ar lines. The binding energies are relative to the vacuum level.

ethylene oxidation [39]. The addition of some copper to these particles has been seen to make the catalytic process more efficient and selective [40, 41]. The mechanism behind this improvement is not fully understood but the spatial distribution of the two components should definitely play an important role in the interaction with the chemicals involved [41].

4.2. Size-dependence of the electronic structure: Papers II & V

As mentioned in chapter 1, the size-dependence of the properties of a nanoscale condensed-matter-system is probably the most central question in fundamental cluster science. The evolution of the energy structure, from metallic towards non-metallic, with a decreasing number of constituent atoms is of great interest within this field [3]. In the present work we have investigated the valence band and the core levels of clusters of tin (paper II) and lead (paper V), two rather "poor" metals that follow the semiconductors silicon and germanium in group IV of the periodic table.

For tin the 4d core level and the 5p valence band in clusters containing from a few tens to a few hundreds of atoms have been probed. The tin clusters have been produced using the EXMEC source with the induction-

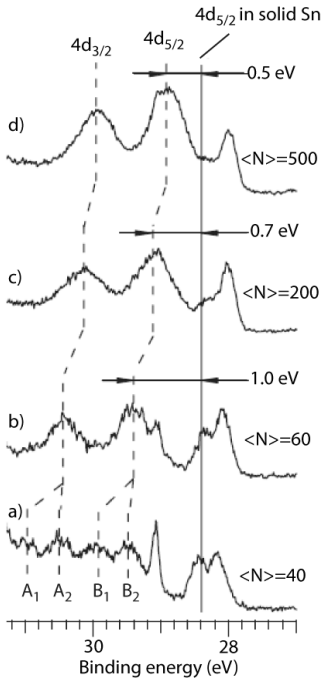

Figure 4.4. Photoelectron spectra of the 4d core level of clusters containing around 40 (a), 60 (b), 200 (c) and 500 (d) atoms. The binding energies are relative to the vacuum level.

heating oven. The different cluster sizes (mean number of constituent atoms estimated by the metal sphere approximation) of ~40, 60, 200 and 500 were achieved by varying the Ar cluster size and the oven temperature. The recorded spectra are shown in figures 4.4 (4d region) and 4.5 (valence region).

Apart from the signal from tin clusters the binding energy region presented in figure 4.4 contains a few other features. The two peaks (of which one becomes too weak to be seen for larger clusters) just above 28 eV are due to the 3s bulk and surface response in Ar clusters. The 3s level signal of Ar atoms (clearly resolved in a) and b)) overlaps with the Sn cluster peaks which can be seen from roughly 29 eV and above. If we first look at the spectrum for Sn clusters of ~500 atoms we observe two peaks at ~28.9 eV and ~30.0 eV. These two peaks are due to the spin-orbit split states of tin clusters, $4d_{5/2}$ (lowest binding energy) and $4d_{3/2}$, separated by 1.1 eV. Each of them contains unresolved bulk and surface contributions. The corresponding position of the $4d_{5/2}$ peak in macroscopic solid tin is at 28.4 eV, i.e. the cluster signal is shifted by ~0.5 eV towards higher binding energies compared to the "infinite" solid case. As the cluster size decreases, the two peaks can be seen to shift further away from the macroscopic solid energy. The most drastic change comes as we produce the smallest clusters (spectrum a)).

For these clusters there are instead four peaks, denoted A_1, A_2, B_1 and B_2. First one can note that the 1.1 eV spin-orbit splitting established for the larger clusters and for the solid, is present also here, namely between peaks A_1 and B_1, and between peaks A_2 and B_2. The peaks of index 2 are found at binding energies ~0.2 eV higher than the peaks for the clusters of 60 atoms seen in spectrum b). We assign these two peaks with the same 1.1-eV spin-orbit splitting as for all the larger clusters, to be the response of smaller metallic clusters shifted up in binding energy due to the decrease in size. With such an assignment the cluster size can then be estimated to ~40 constituent atoms. The index 1 peaks, being separated from each other by the same 1.1 eV, are likely to be another spin-orbit split 4d doublet, but at ~0.5 eV higher binding energy. The presence of this extra pair of peaks can be sought in the produced size distribution. One of the suggestions can be that two specific cluster sizes may be significantly more stable than those in between them. This is however unlikely as mass spectroscopy measurements on tin cluster beams [42-44, and refs. therein] show no such differences in cluster stability. Instead we explain the extra features by differences in electronic structure between two groups of clusters in the beam, which has a certain distribution of sizes. From earlier photoelectron spectroscopy experiments on valence levels [42-44] it is known that the transition from non-metallic to metallic properties occurs in this size range. One can from this propose that for a part of the produced size distribution we have reached a cluster size where the electronic structure is no longer metallic. In a non-metallic system the screening of the created core-hole is not complete, which leads to an abrupt change (increase) in binding energy. In principle, apart from this final-state difference, the observed change in binding energy could also be the result of the differences in the cohesive energy for clusters of different sizes. For various isomers realized in the self-assembling process of cluster formation there might be two prevailing bonding energy values. However, from theoretical considerations on lead clusters [45], one can expect that any significant changes of cohesive energy with decreasing size should happen only at even smaller sizes—below $N \approx 10$.

For the three larger cluster sizes, we probed also the 5p valence band, under the same conditions as for the 4d level, presented as cases b, c, and d of figure 4.4. As can be seen in figure 4.5, the onset of the valence band, mapped by photoelectron spectroscopy, is shifting upwards in binding energy with decreasing size, in a similar way as the 4d features. The cluster work functions, calculated by adding the cluster 4d core-level shift to the work function of the macroscopic solid, have been marked as vertical lines in the figure. A qualitative agreement between these calculated work functions and the actual 5p-band is observed. It means that when the clusters are metallic, the core-level energies measured relative to the cluster Fermi edge (on-set of the valence band) are similar (at least with the accuracy of the present

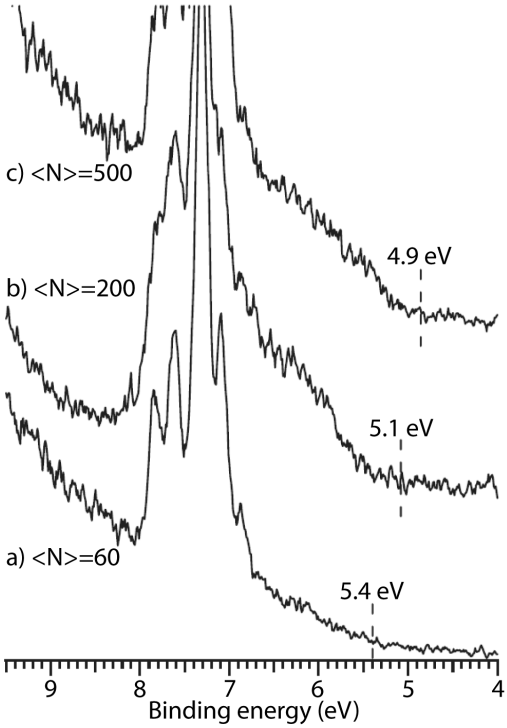

Figure 4.5. Photoelectron spectra of the 5p valence band of clusters containing around 60 (a), 200 (b) and 500 (c) atoms. The binding energies are relative to the vacuum level.

experiment) for all cluster sizes and are close to the corresponding macroscopic solid value.

In similar experiments on Pb clusters we have looked at the 5d core level and the 6p valence level. Using the pick-up source we have produced clusters ranging in size from ~80 atoms and down to 30 and below. The recorded spectra are displayed in figure 4.6 (E-A) below. The left panel shows the $5d_{3/2}$ feature in which, like for tin, the bulk-surface splitting is too small to be resolved (~0.2 eV for solid lead). The right panel shows corresponding valence-region spectra for some of the clustering conditions for which the 5d spectra have been recorded. For comparison we have also included a spectrum of larger clusters, with a mean number of constituent atoms of $\sim 10^4$, produced using the gas-aggregation source (spectrum F). A general trend can be immediately identified; the spectral features shift downwards in energy with increasing size. Furthermore, at smaller sizes one notices that the 5d feature broadens, and in the spectrum of clusters with a mean number of constituent atoms of ~30, a shoulder (feature C_2) towards higher binding energies appears. In the spectra of the smallest clusters two separate maxima (B_1, B_2 & A_1, A_2), being ~0.4 eV from each other, can be observed. This can be interpreted in the same way as for Sn; when we go down in size, below 30

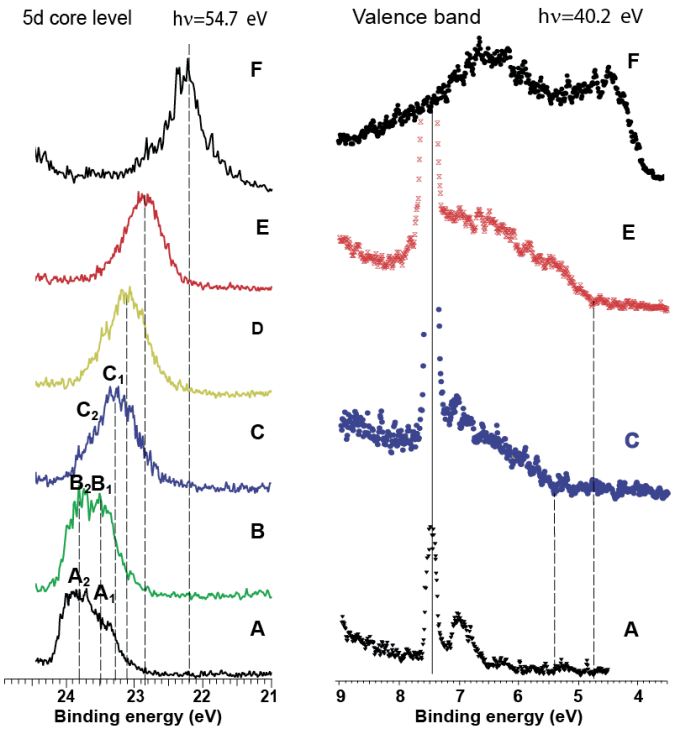

Figure 4.6. Photoelectron spectra of lead clusters of different mean numbers of constituent atoms; ≤ 30 (spectrum A and B), ~30 (C), ~40 (D), ~80 (E), and ~10^4 (F). The left panel displays spectra of the 5d core level while the right panel shows the valence band. Absolute calibration has been done using atomic Pb lines (spectra A-E) and atomic argon lines (spectrum F). The binding energies are relative to the vacuum level.

atoms the smaller clusters in the size distribution of the beam will no longer be metallic and the much less efficient screening of the core-holes in these clusters will cause an increase in binding energy, shifting their spectral response (B_2 and A_2) away from the response of the larger, still metallic, clusters (B_1 and A_1). This is in agreement with theoretical calculations [45] that predict a transition from metal to non-metal at around 20 atoms, with a geometric and electronic structure similar to that of semiconductors Si and Ge in the non-metallic clusters. This structure is claimed to be present for clusters of 22 atoms and less, while the structure of the macroscopic solid co-exists down to 14 atoms [45]. Also, experiments on negatively charged Pb clusters performed with a free-electron laser have shown a comparably large change in binding energy to occur below 20 atoms [46].

For the valence spectra in the right panel of figure 4.6, one can note an up-shift in binding energy with decreasing cluster size for the on-set of the valence band. The shape of the band is also observed to change; when going down in size the width becomes gradually smaller. It is interesting to note

that for clusters of about 80 atoms (spectrum E) with a valence band width ~25% smaller than for the largest clusters, there is no sign of non-metallic clusters in the corresponding 5d spectrum. The features due to such non-metallic clusters cannot be clearly detected until we reach sizes of less than 30 atoms (spectrum A and B), when the corresponding valence band has narrowed to below 25% of the band-width of the macroscopic solid. For the clusters of intermediate sizes (spectrum C, ~30 atoms), for which we approach the transition region, the valence band has approximately half the width compared to the "infinite" solid band and here we see only a shoulder, C_2, hinting about a deviation from metallicity.

To summarize, when the cluster size decreases, we observe in our photoelectron spectra features suggesting non-metallic electronic structure. As mentioned in the beginning of this section, tin and lead are both rather poor metals and belong to group IV of the periodic table, in periods 5 and 6, respectively. The two lighter elements in the same group, in periods 3 and 4, are the semiconductors silicon and germanium. In view of this it is perhaps not surprising that the overlap between the valence and conduction bands disappears when the number of atoms becomes small and the bands become narrower.

4.3. Plasmons in free metal clusters: Papers III & IV

Plasmons are a condensed matter phenomenon where the valence electron density is excited into quantized vibrations relative to the ion lattice of the system. In the work presented in this thesis, the bulk and surface plasmons of free nanoscale Na, K, Mg (Paper III) and Al (Paper IV) clusters have been studied using photoelectron spectroscopy. The outer-most core levels (2p for Na, Mg and Al, 3p for K) have been probed over an extended binding energy interval to include kinetic-energy-loss features due to plasmon excitation. For Na and K, due to the comparably low excitation energy, we have been able to record not only the single-quantum excitations but also the features corresponding to energy losses to two plasmon quanta. The latter have been out of reach for magnesium and aluminium clusters, since these elements have considerably higher plasmon excitation energies. At the same time, this fact should also make the detection of any deviation of the plasmon energies from the corresponding solid-state energies more reliable.

Typical photoelectron spectra are shown in figure 4.7, with the peaks corresponding to the core-level main features and to the plasmon loss-features. Since the plasmon features appear on top of an unknown and complex background, determining the loss-feature positions by fitting over the entire energy range has been difficult. To circumvent this problem we have fitted selected, shorter energy intervals, one at a time, approximating the backgrounds as straight lines within each interval. This approach does not give

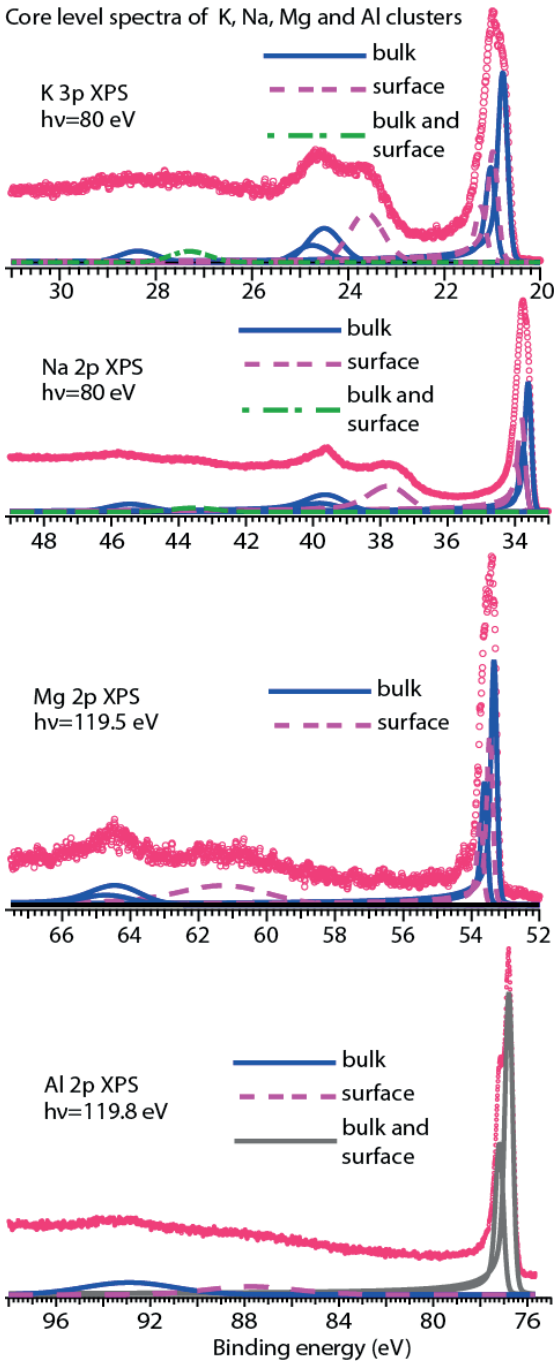

Figure 4.7. Typical photoelectron spectra of the core levels of, from top to bottom, K, Na, Mg , and Al clusters, with the fits. The energy intervals with the main features, the energy loss features corresponding to excitation of one plasmon quantum, and the features corresponding to excitations of two quanta, have been fitted separately. The details of these fittings are shown for Na, as an example, in figure 4.8.

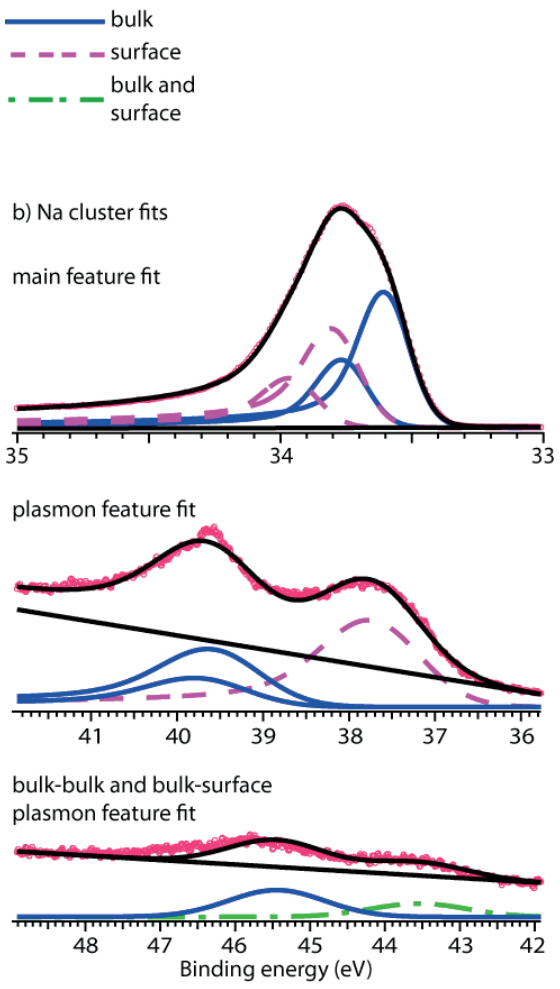

Figure 4.8. The separate fittings are shown for Na, as an example. The resulting curves have then been inserted into the Na overview spectra in figure 4.7. The binding energies are relative to the vacuum level.

accurate relative intensities for the plasmon peaks, but provides reasonable peak positions, especially considering that the plasmon peaks are broad and that some of them are well separated. As an example, the fitting results for the three different energy intervals of Na clusters are shown in figure 4.8. The clusters are, using the metal sphere approximation, estimated to have mean radii of ~5 nm (K), ~3 nm (Na), amply 10 nm (Mg) and 3-4 nm (Al).

For the elements of paper III, the main features could be assigned and described well under the assumption of the same subcomponents and spectral characteristics as for the macroscopic solids of the same materials, with four peaks corresponding to bulk and surface contributions of two spin-orbit split states. In the case of Al, the bulk-surface splitting is too small to motivate the use of separate peaks for these two sites for each spin-orbit component,

so only one peak for each spin-orbit state has been used in the fitting. Under the assumption that all photoelectrons can excite surface plasmons while bulk-plasmon excitations are mostly caused by bulk photoelectrons, the bulk and surface plasmons are expected to consist of two and four peaks respectively. Since the spin-orbit and bulk-surface splittings are small compared to the plasmon peak widths observed in the present work, we have, for Na, K and Mg, chosen to fit the plasmon features due to the energy losses for single-quantum plasmon excitations with three peaks: two spin-orbit peaks for the bulk and one common for the four possible surface plasmon contributions. For Al we have limited ourselves to one peak for the bulk and one for the surface.

At the macroscopic scale, in a number of metals, additional energy loss features have been observed and interpreted as arising from harmonic excitations of plasmon overtones. In our work, for K and Na clusters, we have observed features in the energy regions corresponding to the overtones. Assuming that also these peaks are due to the harmonic overtone excitation, one could expect two peaks, one of them separated from the main feature by twice the surface plasmon energy E_{sp} ("surface-surface" plasmons) and the other one by twice the bulk plasmon energy E_{bp} ("bulk-bulk" plasmons). Indeed, at around the energy where the bulk-bulk plasmons are expected spectral features have been observed for K and Na clusters. However, no peaks could be seen where the surface-surface plasmons have been expected. Instead there is a peak separated from the main feature by the sum of one bulk and one surface plasmon quanta ("bulk-surface" plasmon). Features of this latter kind have typically not been observed for the planar sample case and are unlikely to be the result of harmonic excitation. Their presence indicates the occurrence of sequential excitations, which may also contribute significantly to the bulk-bulk plasmon peaks. In the fitting procedure, these bulk-bulk and bulk-surface peaks have been given fixed energies at a corresponding separation from the main features and peak widths that appeared reasonable.

The observed plasmon energies are in all cases found to be rather close to the experimental values for the planar macroscopic samples of the same materials. The good agreement between the values given by the Drude-model formulas and the experimental macroscopic solid values, and the measured cluster values in our experiments suggest that the electronic densities in clusters of the actual sizes are close to the solid state densities. This can be seen as an additional confirmation of cluster metallicity.

Interestingly, there is a clear difference in the surface plasmon energy between the cases of optical excitation and excitation due to core-hole ionization of free metal clusters. Most investigations of plasmons in free clusters have been done by measuring the optical absorption in search of resonances. While mainly smaller clusters have been probed, Bréchignac and co-workers have studied surface plasmons in clusters in a size range up ~900 atoms [47].

They found the plasmon excitation energies to be all the time smaller than the Mie resonance, of energy $E_{Mp} = E_{bp} / \sqrt{3}$, and to be increasing towards this energy with increasing size. For macroscopic planar surfaces, theory claims that the surface plasmon excitation energies should instead have the value we have observed in this work, $E_{sp} = E_{bp} / \sqrt{2}$, both for optical and the electron scattering excitation [22, 48]. The question arises then why, for these particles, the response of electron density is different to optical absorption and core-level ionization? Or more specifically; why is it that at the spherical surfaces of clusters, the external electromagnetic field (optical radiation) excites collective electron oscillations with a frequency around the Mie resonance or below, while the internal field—due to the electron–hole pair appearance—causes electron oscillations with a frequency close to that of the planar solid?

5. Summary & Outlook

Using synchrotron radiation-based photoelectron spectroscopy the electronic structure of free clusters of several metallic elements has been investigated. All experiments have been performed at the soft x-ray beamline I411 at the MAX II storage ring at MAX-lab. The studied clusters have been produced using two different cluster sources, a gas-aggregation source (for the larger clusters in papers I, III, IV and VI) and a pick-up source (for the smaller clusters in papers II and V). From the recorded photoelectron spectra various information about 1) surface segregation in self-assembled nanoalloy (NaK, CuAg) clusters (papers I and VI), 2) size-dependence of the electronic structure and the development of metallicity in tin and lead clusters (papers II and V), and 3) the excitation of plasmons in sodium, magnesium, potassium and aluminium clusters (papers III and IV) has been derived.

Surface segregation in free self-assembled clusters has been observed earlier for various noble gas mixtures. Noble gas clusters have frequently been seen as simple model systems for other clusters that may have closer connections to applications [4]. As a next step after the inert-gas clusters we have addressed the clusters formed from a mixture of Na and K vapours. From the Na 2p and K 3p core-level photoelectron spectra we have been able to conclude that mixed NaK nanoalloy clusters were formed, with a clearly potassium-dominated surface and a mixed sodium-potassium bulk. The K surface dominance holds even when the clusters contain over 60% sodium. This finding is in line with theory which says that the surface sites are more likely to be occupied by atoms of the largest size and lowest cohesive energy—K fulfils both conditions. We have made a similar investigation of clusters condensed from mixed vapours of silver and copper. Also here the recorded spectra suggest that the clusters assume a core-shell structure with the surface consisting mainly of the element with lowest cohesive energy and largest atoms, i.e. silver, and a mixed bulk. This possibility to investigate the structure of clusters consisting of more than one type of atoms can, of course, be used also for the clusters where the different types of constituent atoms are not as similar as for those studied so far. First results of this kind have been obtained both for clusters formed from a vaporized CdS target and for clusters formed from lead-atom vapour in an oxygen atmosphere.

The development of metallicity in tin clusters with increasing size has previously been addressed using valence photoelectron spectroscopy, and has, for initially negatively charged clusters, been found to occur already for

clusters of ~40 atoms. We have probed the 4d core level of neutral Sn clusters with mean numbers of constituent atoms of approximately 40, 60, 200 and 500 atoms. The photoelectron spectra of the clusters of the three largest mean sizes display spectral features implying that the clusters have assumed an electronic structure similar to the metallic solid state. For the clusters containing around 40 atoms, the spectrum contains additional features suggesting that a part of the produced cluster size distribution is instead in a non-metallic phase. The occurrence of this phase transition at around this size is in agreement with the above mentioned valence band studies. From our experiments the difference in binding energy for these two phases is approximately 0.5 eV. Additionally we have probed the 5p valence band for the three largest sizes and noted that the work functions derived from the core level spectra agree fairly well with the minimum ionization energies (on-sets of the valence bands) which provides additional confirmation for the validity of the metallicity assumption for these sizes. In our experiments on lead clusters in the size range below 100 atoms we start to see this kind of additional features, interpreted to correspond to another, non-metallic phase, when we go below 30 atoms in size. This observation is in agreement both with theoretical considerations suggesting a transition from a metallic to a non-metallic state at ~20 atoms and with free-electron-laser experiments where non-metallic clusters were seen for sizes below 20. After tin and lead, a natural direction to proceed is to investigate the energy structure size-dependence of other group 14 elements like silicon and germanium. Since the latter two are semiconductors, such a drastic change as a metal-to-non-metal transition cannot be expected but there could still be observable changes in the electronic structure. For example, some photoelectron spectroscopy studies of the valence levels suggest silicon clusters to have a much larger band gap than macroscopic Si [49].

The nature of plasmon excitations as a result of photoionization has been investigated for free clusters out of sodium, potassium, magnesium and aluminium atoms. Until recently, the studies of plasmons in free clusters have mainly been performed using optical absorption. With this method, the value of the Mie absorption resonance can be derived but the study of bulk plasmons is problematic. The bulk plasmons have however been studied in macroscopic solids using photoelectron spectroscopy. Here, for the planar solids, not only signals due to the excitation of single-quantum plasmons but also features corresponding to harmonic plasmon overtone excitation have been observed. Our group has earlier managed to implement the photoelectron spectroscopy technique in the studies of plasmons in free clusters and record spectra with both bulk and surface plasmon features in potassium clusters [30]. As a next step we have extended our studies in this field, not only to bulk and surface plasmon in the clusters of additional elements, sodium, magnesium and aluminium, but also to plasmon features corresponding to the excitation of more than one plasmon quantum. As previously for potassi-

um, we found that also for Na, Mg and Al, both the bulk and surface excitation energies are very similar to the energies measured for the macroscopic solid case. Interestingly, we see no sign of plasmon excitation of the energies corresponding to the Mie resonance. For K and Na clusters we have observed features corresponding to the excitation of two bulk plasmon quanta and to one bulk and one surface quantum. While the "bulk-bulk" plasmons can be explained by a harmonic overtone excitation, the presence of the "bulk-surface" plasmons indicates the occurrence of sequential plasmon excitation. This means that such sequential processes are possibly involved, to a not insignificant extent, also in the case of the "bulk-bulk" plasmon excitation. As a continuation of our plasmon studies we hope to be able to observe plasmon features also for smaller clusters, produced with the pick-up source. This with the aim of investigating how far down in size the plasmon excitation energies remain the same as in the corresponding macroscopic solids.

Acknowledgments

The work presented here has been performed over the course of several years. It is the result of the cooperation between a large number of people at a number of different institutes who have contributed in varying degree to the development of experimental equipment, the collection and analysis of data and the communication of the results. Mainly, this includes colleagues at the Department of Physics and Astronomy, Uppsala University; the Department of Synchrotron Radiation Research, Lund University; the Department of Physics, University of Oulu; and MAX-lab. I would like to thank specifically my supervisors Olle Björneholm and Maxim Tchaplyguine for their guidance through my PhD studies and also the staff at the Department of Physics and Astronomy, Uppsala University and MAX-lab for their assistance in various matters.

Summary in Swedish: Fria metallkluster studerade med fotoelektronspektroskopi

Klusterfysik

Ett kluster är i det aktuella fysikaliska sammanhanget en partikel bestående av ett ändligt antal atomer. Innehåller kluster endast ett fåtal atomer har det egenskaper liknande enskilda atomer eller molekyler. Om antalet ingående atomer är väldigt stort börjar egenskaperna istället likna dem hos det fasta tillståndet. Lägger man till fler och fler atomer till ett litet kluster kommer man alltså se en förändring av klustrets egenskaper mot det fasta tillståndets. Den centrala frågan inom klusterfysik är kartläggningen av detta storleksberoende. I detta arbete har elektronstrukturen hos kluster studerats med hjälp av synktrontronljusbaserad fotoelektronspektroskopi.

Elektronstruktur

Elektroner i en atom är ordnade i ett antal diskreta energinivåer, som kan sägas omge atomkärnan. De yttersta av dessa kallas valensnivåer och det är i huvudsak elektronerna i dessa som avgör atomens kemiska och fysikaliska egenskaper som t.ex. hur den binder sig till andra atomer och formar molekyler, fasta objekt, eller kluster. Elektronerna i de inre energinivåerna har inte samma direkta påverkan på atomens beteende men de bär likväl på intressant information om atomen och dess omgivning. I molekyler är elektronstrukturen väldigt lik den hos atomer. Skillnaden ligger främst hos valensnivåerna. De har fortfarande specifika energier men tillhör ej längre en enskild atom utan är gemensamma för hela molekylen. I små kluster bestående av några få atomer är situationen densamma, fast antalet tillåtna valensnivåer är fler. Efterhand som klusterstorleken ökar kommer dessa nivåer att bli fler och fler för att så småningom överlappa och ge upphov till så kallade energiband. Det är den här typen av elektronstruktur som återfinns hos fasta objekt. De inre energinivåerna behåller dock sin atomlika natur oavsett storleken på objektet de tillhör.

Elektronstrukturen är vad som avgör om ett ämne är en metall eller inte. Utanför valensbandet finns det ytterligare, tomma, band. Om det närmaste av dessa band, det så kallade ledningsbandet, överlappar med valensbandet är

ämnet en metall. Ett sådant överlapp låter valensbandets elektroner övergå till ledningsbandet där de fritt kan röra sig genom ämnet, vilket ger metaller deras typiska förmåga att leda ström. Om banden inte överlappar utan har ett gap mellan sig finns normalt ingen sådan ledningsförmåga och ämnet är då en isolator (eller en halvledare om gapet är litet). Om ett kluster av ett metalliskt ämne blir väldigt litet kommer inte valensnivåerna att vara tillräckligt många för att ge upphov till lika breda band. Ett gap kan då uppstå och klustret blir en isolator.

Det faktum att valenselektronerna i ett fast objekt är gemensamma för hela objektet kan de också reagera kollektivt på ett sätt som vore omöjligt om de ingående atomerna ej var bundna till varandra, som i en gas. Ett exempel på ett sådant kollektivt agerande från elektronernas sida är så kallade plasmoner, som kan uppstå till följd av t.ex. fotojonisering. Dessa kan enklast beskrivas som en sorts vågrörelser som uppstår i ett objekt till följd av att det utsätts för elektromagnetiskt fält. En enkel mekanisk motsvarighet är vågorna som orsakas av att en sten släpps i en sjö.

Fotoelektronspektroskopi

Fotoelektronspektroskopi är en experimentell teknik baserad på den fotoelektriska effekten. När en foton (ljuspartikel) träffar ett föremål kan den absorberas av detta. Fotonens energi överlämnas då till föremålet. Om fotonen har en tillräckligt hög energi kan föremålet joniseras. Det innebär att en elektron slits loss och skickas ut från föremålet. Detta kallas fotojonisering. Den energi som inte går åt för att lösgöra elektronen från föremålet överförs som rörelseenergi till elektronen. Om man vet fotonens energi kan man, om man mäter elektronens rörelseenergi, räkna ut elektronens bindningsenergi, d.v.s. energin som krävdes för att slita loss den. En elektrons bindningsenergi beror på till vilkens sorts atom den är bunden och i vilket skal inom atomen den befinner sig. Dessutom påverkas den av sin värdatoms kemiska omgivning (har den andra atomer omkring sig och i så fall ur många och vilka sorter?).

I ett fotoelektronspektroskopiskt experiment sänder man in ett stort antal fotoner mot ett föremål och mäter de utkommande elektronernas energifördelning (antalet elektroner av varje energi). Resultatet blir ett fotoelektronspektrum. Från ett sådant spektrum kan man dra slutsatser om vilka atomer föremålet består av och hur de är fördelade inom föremålet m.m. Fotoelektroner får olika energier beroende på från vilken sorts atom de kommer ifrån, var atomen är placerad (på ytan eller i innandömet), hur effektivt det positivt laddade objekt den lämnar efter sig skärmar sin positiva laddning, om den ger upphov till en plasmon, etc. Därmed kan sådana detaljer undersökas med hjälp av denna metod.

Synkrotronljus

I det här arbetet har elektronstrukturen hos kluster studerats med hjälp av synkrotronljusbaserad fotoelektronspektroskopi. Synkrotronljus är en typ av strålning som uppstår när elektriskt laddade partiklar (i det här fallet elektroner), som färdas i hastigheter nära ljusets, accelereras. I en synkrotrotronljusanläggning låter man elektroner färdas genom magnetiska fält för att få dem att ändra riktning. De ger då ifrån sig synktrontronljus som har flera användbara egenskaper. Strålningen kommer att vara väl kollimerad, d.v.s. allt ljus kommer att färdas i samma riktning som hos en laser och inte åt alla hall som ljuset från en glödlampa. Detta gör att allt ljus kan utnyttjas. Strålningen kommer att vara monokromatisk, vilket betyder att alla fotoner (ljuspartiklar) kommer att ha, så gott som, samma energi (samma våglängd, ”färg”). Även detta är en egenskap som delas av lasrar, medan många andra ljuskällor istället sänder ut strålning med ett brett spektrum av energier. Då varje ljusenergi ger upphov till olika energier hos de utkommande elektronerna så skulle ett spektrum uppmätt med en sådan ”flerfärgad” ljuskälla göra det svårt, ofta omöjligt, att dra några slutsatser. Synktronljusets fördel framför lasern är framförallt de tillgängliga energierna. En typisk laser ger ifrån sig en specifik energi, vill man ha en annan energi får man byta lasersystem. Vilken laser man än väljer kan aldrig nå djupare i elektronstrukturen än till valensnivåerna. På en synkrotronljusanläggning kan man fritt välja energi i ett brett interval och framförallt kan man nå långt högre energier än med en laser. Därmed blir även de djupare energinivåerna tillgängliga för spektroskopiska undersökningar.

Resultaten av detta arbete

Tre saker har studerats:

1. Om kluster produceras av atomer av två olika ämnen, hur kommer de olika atomerna att formera sig inom klustret?

2. Klustrens egenskaper förändras med storleken. Vid vilken storlek kommer kluster av metalliska grundämnen att förlora sina metalliska egenskaper?

3. Hur påverkas plasmonerna av klustrens storlek?

I vårt arbete med den första punkten har vi producerat kluster av natrium och kalium och av koppar och silver. Vi har i båda fallen funnit klustren antar en segregerad struktur, med en yta som domineras av ett av ämnena och ett inre bestående av båda. Detta har vi kunnat avgöra genom fotoe-

lektronspektroskopins förmåga att särskilja elektronsignalerna från ytan och innandömet. Vilka ämnen som hamnar på ytan (natrium och silver) avgörs av atomstorleken men även av atomernas olika benägenhet att binda sig till sin omgivning.

För att studera de metalliska egenskaperna hos små kluster har vi producerat kluster av tenn och bly av en rad olika storlekar. När antalet atomer i klustren blir så få som några tiotal (under 40 för tenn, under 20-30 för bly) ser vi tydliga tecken på att bandgap uppstått i klustren. P.g.a. detta får fotoelektronerna får en annan energi vilket gör att de förskuts i spektrumet.

Även när fotojoniseringen ger upphov till en plasmon, förskjuts fotoelektronen. Denna förskjutning är av samma storlek som denna energi som krävs för att orsaka vågrörelsen. För att undersöka hur denna energi påverkas när storleken minskar har vi studerat förskjutningen för kluster av natrium, kalium, magnesium och aluminium bestående av ~1000 atomer eller mer. Vi har sett att energierna fortfarande är desamma för dessa partiklar med radier på bara några få nanometer.

Sammanfattning

Med hjälp av synkrotronljusbaserad fotoelektronspektroskopi har vi har vi studerat egenskaper hos kluster som är intressanta för vår grundläggande förståelse för hur fasta objekts egenskaper utvecklas med antalet ingående atomer. Just detta storleksberoende hos klustren gör dem dock intressanta även från ett mer tillämpat perspektiv. En möjlighet är att användas kluster av vissa utvalda storklerkar, och därmed vissa utvalda egenskaper, som byggstenar i nya material. Till exempel används nanopartiklar av silver som katalysatorer för oxidering av etylen. Dessa har funnits bli mer effektiva om man tillsätter små mängder koppar. En viktig detalj hos dessa nanolegeringar är hur atomerna från de olika ämnena är ordnade i förhållande till varandra, vilket är en av anledningarna för våra studier av kluster producerade av koppar och silver.

Bibliography

1. H. Haberland (ed.), Clusters of Atoms and Molecules I & II, Springer Ser. Chem. Phys. **52** Springer, Berlin, (1994-1995).

2. R. Busani, M. Folkers, O. Cheshnovsky, Phys. Rev. Lett. **81**, 3836 (1998).

3. B. von Issendorff, O. Cheshnovsky, Annu. Rev. Phys. Chem. **56**, 549 (2005).

4. K. D. Sattler (ed.), Handbook of Nanophysics, CRC Press; 1st edition (2010).

5. G. K. Wertheim, Phase Transitions **24-26**, 203 (1990).

6. G. Wrigge, M. Astruc Hoffmann, B. v. Issendorff, Phys. Rev. A **65**, 063201 (2002).

7. S. Peredkov, G. Öhrwall, J. Schulz, M. Lundwall, T. Rander, A. Lindblad, H. Bergersen, A. Rosso, W. Pokapanich, N. Mårtensson, S. Svensson, S. L. Sorensen, O. Björneholm, M. Tchaplyguine, Phys. Rev. B **75**, 235407 (2007).

8. C. Zhang, T. Andersson, S. Svensson, O. Björneholm, M. Huttula, M.-H. Mikkelä, M. Tchaplyguine, G. Öhrwall, J. Chem. Phys. **134**, 124507 (2011).

9. M. Tchaplyguine, S. Peredkov, H. Svensson, J. Schulz, G. Öhrwall, M. Lundwall, T. Rander, A. Lindblad, H. Bergersen, S. Svensson, M. Gisselbrecht, S. L. Sorensen, L. Gridneva, N. Mårtensson, O. Björneholm, Rev. Sci. Inst. **77**, 033106 (2006).

10. H. Haberland, M. Mall, M. Moseler, Y. Qiang, Th. Reiners, Y. Thurner, J. Vac. Sci. Technol. A **12**, 2925 (1994).

11. http://www.thermocoax.com/ 13/10-2012.

12. http://www.ajaint.com/whatis.htm 13/10 - 2012.

13. S. Peredkov, Free clusters studied by synchrotron-based x-ray spectroscopy: From rare gases to metals, Lund University (2007).

14. M. Schmidt and H. Haberland, Eur. Phys. J. D **6**, 109 (1999).

15. M. Huttula, M.-H. Mikkelä, M. Tchaplyguine, O. Björneholm, J. Electron Spectrosc. Relat. Phenom. **181**, 145 (2010).

16. O. F. Hagena, W. Obert, J. Chem. Phys. **56**, 1793 (1972).

17. N. Mårtensson, P. Baltzer, P. A. Brühwiler, J.-O. Forsell, A. Nilsson, A. Stenborg, B. Wannberg, J. Electron Spectrosc. Relat. Phenom. **70**, 117 (1994).

18. J. J. Yeh, I. Lindau, Atomic Data and Nuclear Data Tables **32**, (1985).

19. A. Kikas, S. J. Osborne, A. Ausmees, S. Svensson, O.-P. Sairanen, S. Aksela, J. Electron Spectrosc. Relat. Phenom. **77**, 241 (1996).

20. G. K. Wertheim, D. M. Riffe, Phys. Rev. B **52**, 14906, 1995.

21. S. Doniach, M. Šunjić, J. Phys. C: Solid St. Phys. **3**, 285 (1970).

22. N. W. Ashcroft, N. D. Mermin, Solid State Physics, Harcourt, Orlando, FL (1976).

23. S. Hüfner, Photoelectron Spectroscopy, Springer Verlag, Germany, (1995).

24. P. Steiner, H. Höchst, S. Hüfner, Z. Phys. B **30**, 129 (1978).

25. G. Pirug, A. Winkler, and H. P. Bonzel, Surf. Sci. **163**, 153 (1985).

26. G. Makov, A. Nitzan, L. E. Brus, J. Chem. Phys. **88**, 5076 (1988).

27. G. Mie, Ann. Phys. **330**, 377 (1908).

28. C. Xia, C. Yin, and V. V. Kresin, Phys. Rev. Lett. **102**, 156802 (2009).

29. K. Kolwas, S. Demianiuk, and M. Kolwas, J. Phys. B **29**, 4761 (1996).

30. A. Rosso, G. Öhrwall, I. Bradeanu, S. Svensson, O. Björneholm, M. Tchaplyguine, Phys. Rev. A **77**, 043202 (2008).

31. R. Schlipper, R. Kusche, B. von Issendorff, and H. Haberland, Phys. Rev. Lett. **80**, 1194 (1998).

32. E. Kukk, Spectral Analysis by Curve Fitting Macro Package /SPANCF/ 2000.

33. M. Lundwall, H. Bergersen, A. Lindblad, G. Öhrwall, M. Tchaplyguine, S. Svensson, O. Björneholm, Phys. Rev. A **74**, 043206 (2006).

34. M. Lundwall, M. Tchaplyguine, G. Öhrwall, R. Feifel, A. Lindblad, A. Lindgren, S. Sörensen, S. Svensson, O. Björneholm, Chem. Phys. Lett. **392**, 433 (2004).

35. M. Lundwall, W. Pokapanich, H. Bergersen, A. Lindblad, T. Rander, G. Öhrwall, M. Tchaplyguine, S. Barth, U. Hergenhahn, S. Svensson, O. Björneholm, J. Chem. Phys. **126**, 214706 (2007).

36. S. Peredkov, G. Öhrwall, J. Schulz, M. Lundwall, T. Rander, A. Lindblad, H. Bergersen, A. Rosso, W. Pokapanich, S. Svensson, S. L. Sorensen, N. Mårtensson, O. Björneholm, M. Tchaplyguine, Phys. Rev. B **75**, 235407 (2007).

37. M. Schick, G. Ceballos, Th. Pelzer, J. Schafer, G. Rangelov, J. Stober, K. Wandelt, J. Vac. Sci. Technol. A **12**, 1795 (1994).

48. R. Ferrando, J. Jellinek, R. L. Johnston, Chem. Rev. (Washington, D.C.) **108**, 845 (2008)

39. B. Hodnett, Heterogeneous Catalytic Oxidation, John Wiley and Sons, Ltd., Chichester, U.K. (2000).

40. J. T. Jankowiak, M. A. Barteau, J. Catal. **236**, 366 (2005).

41. S. Piccinin, S. Zafeiratos, C. Stampfl, T. W. Hansen, M. Hävecker, D. Teschner, V. I. Bukhtiyarov, F. Girgsdies, A. Knop-Gericke, R. Schlögl, M. Scheffler, Phys. Rev. Lett. **104**, 035503 (2010).

42. S. Yoshida, K. Fuke, J. Chem. Phys. **111**, 3880 (1999).

43. L.-F. Cui, L.-M. Wang, L.-S. Wang, J. Chem. Phys. **126**, 064505 (2007).

44. Y. Negishi, H. Kawamata, A. Nakajima, K. Kaya, J. Electron Spectrosc. Relat. Phenom. **106**, 117 (2000).

45. B. Wang, J. Zhao, X. Chen, D. Shi, G. Wang, Phys. Rev. A **71**, 033201 (2005).

46. V. Senz, T. Fischer, P. Oelßner, J. Tiggesbäumker, J. Stanzel, C. Bostedt, H. Thomas, M. Schöffler, L. Foucar, M. Martins, J. Neville, M. Neeb, Th. Möller, W. Wurth, E. Rühl, R. Dörner, H. Schmidt-Böcking, W. Eberhardt, G. Ganteför, R. Treusch, P. Radcliffe, and K.-H. Meiwes-Broer, Phys. Rev. Lett **102**, 138303 (2009).

47. C. Bréchignac, P. Cahuzac, N. Kebaïli, J. Leygnier, A. Sarfati, Phys. Rev. Lett. **68**, 3916 (1992).

48. A. C. Simonsen, F. Yubero, S. Tougaard, Phys. Rev. B **56**, 1612 (1997).

49. M. Astruc Hoffmann, G. Wrigge, B. v. Issendorff, J. Müller, G. Ganteför, H. Haberland, Eur. Phys. J. D **16**, 9 (2001).

Acta Universitatis Upsaliensis

Digital Comprehensive Summaries of Uppsala Dissertations from the Faculty of Science and Technology 992

Editor: The Dean of the Faculty of Science and Technology

A doctoral dissertation from the Faculty of Science and Technology, Uppsala University, is usually a summary of a number of papers. A few copies of the complete dissertation are kept at major Swedish research libraries, while the summary alone is distributed internationally through the series Digital Comprehensive Summaries of Uppsala Dissertations from the Faculty of Science and Technology.

Distribution: publications.uu.se
urn:nbn:se:uu:diva-183031

ACTA
UNIVERSITATIS
UPSALIENSIS
UPPSALA
2012